Inhibition of PI3K pathway increases immune infiltrate in muscle-invasive bladder cancer

Edith Borcoman, Philippe de La Rochere, Wilfrid Richer, Sophie Vacher, Walid Chemlali, Clémentine Krucker, Nanour Sirab, François Radvanyi, Yves Allory, Géraldine Pignot, et al.

Inhibition of PI3K pathway increases immune infiltrate in muscle-invasive bladder cancer

[*]Borcoman E[1,2], [*]De La Rochere P[2], Richer W[2], Vacher S[3], Chemlali W[3], Krucker C[4], Sirab N[4], Radvanyi F[4], Allory Y[4,5], Pignot G[6], Barry de Longchamps N[7], Diamotte D[8], Meseure D[9], Sedlik C[2], Bièche I[3], Piaggio E[2]

[1] Institut Curie, Department of Medical Oncology, 26 rue d'Ulm, Paris 75005, France.

[2] Institut Curie, PSL Research University, INSERM U932, 26 rue d'Ulm, Paris 75005, France.

[3] Institut Curie, Unit of Pharmacogenomics, Department of Genetics, 26 rue d'Ulm, Paris 75005, France.

[4] Institut Curie, PSL Research University, CNRS UMR 144, 26 rue d'Ulm, Paris 75005, France.

[5] Institut Curie, Department of diagnostic and theranostic medicine, 35 Rue Dailly, Saint-Cloud 92210, France.

[6] Institut Paoli-Calmettes, Department of Urology, Marseille 13009, France.

[7] Hôpital Cochin, Department of Urology, Paris 75014, France.

[8] Hôpital Cochin, Department of Pathology, Paris 75014, France.

[9] Institut Curie, Department of diagnostic and theranostic medicine, 75005, Paris, France.

*B.E. and DLR. P. contributed equally to manuscript.

Correspondence to:

Email: eliane.piaggio@curie.fr

Word Count: Abstract = 222 (max 250) words; Tables = 4; Figures = 6 + 5 supplementary figures; Pages = 45; References = 42

Abstract

Although immune checkpoint inhibitors have shown improvement in survival in comparison to chemotherapy in urothelial bladder cancer, many patients still fail to respond to these treatments and actual efforts are made to identify predictive factors of response to immunotherapy. Understanding the tumor-intrinsic molecular basis, like oncogenic pathways conditioning the presence or absence of tumor-infiltrating T cells (TILs), should provide a new rationale for improved anti-tumor immune therapies.

In this study, we found that urothelial bladder cancer from human samples bearing *PIK3CA* gene mutations were significantly associated with lower expression of a defined immune gene signature, compared to unmutated ones. We identified a reduced-10 genes immune gene signature that discriminates muscle-invasive bladder cancer (MIBC) samples according to immune infiltration and *PIK3CA* mutation. Using a humanized mouse model, we observed that BKM120, a pan-PI3K inhibitor, significantly inhibited the growth of a human bladder cancer cell line bearing a *PIK3CA* mutation, associated to increased immune cell infiltration (hCD45+). Using qRT-PCR, we also found an increase in the expression of chemokines and immune genes in *PIK3CA*-mutated tumors from mice treated with BKM120, reflecting an active immune

infiltrate in comparison to untreated ones. Moreover, addition of BKM120 rendered *PIK3CA*-mutated tumors sensitive to PD-1 blockade. Our results provide a relevant rationale for combination strategies of PI3K inhibitors with immune checkpoint inhibitors to overcome resistance to immune checkpoint inhibitors.

Introduction

Bladder cancer is considered as a major source of mortality worldwide, with an estimate of 429,800 new cases and 165,100 deaths worldwide in 2012[1]. About two-thirds of newly diagnosed urothelial bladder cancers are non-muscle-invasive bladder cancer (NMIBC) that can further evolve to muscle-invasive tumors in about 10% of cases; and one-third of the newly diagnosed cases are muscle-invasive bladder cancer (MIBC)[2]. Despite chemotherapy treatments, the prognosis of metastatic urothelial carcinoma remains poor after the first line platinum-based regimen and there is an urgent need for new effective strategies in this setting[3,4]. Immunotherapy, such as immune checkpoint inhibitors, offers as a new therapeutic option in advanced urothelial carcinoma resulting in survival improvement in comparison to chemotherapy[5,6].

Immunotherapy has made a breakthrough in cancer treatment, in many different types of tumors. However, many patients still fail to respond to immune checkpoint therapies, as only around 20 to 40% of patients will initially respond to those treatments, and some responders will eventually acquire resistance to the treatment and relapse after a period of response[7]. Thus, there is a need to gain knowledge on the mechanism of action of these approaches and overcome resistance.

Response to immune checkpoint inhibitors seems to be conditioned by the infiltration of tumors by activated T cells, evidenced by an ongoing anti-tumor immune response[8–10]. Tumors with a T-cell-inflamed microenvironment, also referred to as “hot tumors”, are characterized by a high $CD8^+$ T cell infiltrate, the expression of chemokines involved in T-cell recruitment[8], and a type-I interferon (IFN) signature, and are associated with improved patient survival and better responses to immunotherapies[8,9,11]. Otherwise, tumors that lack infiltration of activated T cells in the

tumor microenvironment, defined as “cold” tumors, have been described as presenting low or no clinical response to immunotherapies[12].

Efforts are being made to better understand the mechanisms leading to T-cell exclusion or T-cell inactivation in the tumor microenvironment. Hence, understanding the tumor-intrinsic molecular bases, such as oncogenic pathways, dictating the presence or absence of tumor infiltrating T cells (TILs), should provide a new rationale for improved anti-tumor immune therapies.

The PI3K/AKT/mTOR pathway is involved in different cellular functions and regulates cell cycle, cell growth, metabolism, proliferation and survival that are all hallmarks of cancer cells implicated in initial growth and extension of cancer[12]. Genetic alterations, leading to overactivation of the PI3K/AKT/mTOR pathway are frequent events in many types of cancers[13].

The phosphatidylinositol-4,5-bisphosphate 3-kinase catalytic subunit alpha (*PIK3CA)* gene is an oncogene frequently implicated in the overactivation of the PI3K/AKT/mTOR pathway, somatic *PIK3CA* mutations leading to an increase of kinase activity of phosphoinositide 3-kinase (PI3Ks). It has been found that recurrent somatic mutations of *PIK3CA*, known as hotspot mutations, are frequently involved in overactivation of the PI3K/AKT/mTOR pathway in tumors. These hotspot-activating point mutations are frequently detected either on exon 9 (encoding for the helical domain of the protein, E542K and E545K) or on exon 20 (encoding for the kinase domain of the protein, H1047R and H1047L) (COSMIC database). Also, frequent genetic alterations leading to the loss of phosphatase and tensin homolog (PTEN, a tumor suppressor that inhibits PI3K), can result in the overactivation of the PI3K/AKT/mTOR pathway.

Interestingly, Parsa and colleagues described that in human glioma the expression of PD-L1 is increased post transcriptionally after the deletion of PTEN and the activation of the PI3K/AKT/mTOR pathway[14]. It has already been shown in a melanoma model that the loss of PTEN and the consequent activation of the PI3K/AKT/mTOR pathway promotes resistance to T cell-mediated immunotherapy[15].

These molecular events do not explain all the cases of non-T-cell-infiltrated melanomas, and the particular cases of other types of tumors remain to be studied so as to better understand resistance mechanisms to anti-immune checkpoint inhibitors. Along these lines, Sweis and colleagues showed that β-Catenin, PPAR-γ, and FGFR3 pathways were activated in non-T-cell-inflamed bladder tumors, correlating those tumor-intrinsic oncogenic pathways with T-cell exclusion, and thus identifying those pathways as potential targetable pathways of tumor-intrinsic immunotherapy resistance[16].

Therefore in our study, we assessed the correlation between genetic alterations of selected druggable tumor-intrinsic oncogenic pathways and immune cell infiltration in bladder cancer, more specifically in MIBC, so as to provide a new rationale for improved anti-tumor immune therapies in this setting.

Results

Mutation of *PIK3CA* correlates with non-T-cell-inflamed MIBCs

We first evaluated whether bladder tumors could be classified as “T-cell-inflamed” or “non-T-cell-inflamed” by evaluating their immune gene expression profile using quantitative PCR (qRT-PCR). For that, we first defined an immune gene signature, of

57 genes that comprised: i) genes commonly used to identify major immune cell populations described to be present in the human tumor microenvironment[17] (i.e. *FOXP3* to identify Tregs, see **Table 1** for the complete list), ii) a selection of immunomodulatory genes comprising druggable immune checkpoints (in clinical use or under evaluation) and including at least one member of the most studied families[18], and iii) major histocompatibility complex (MHC) genes (*HLA* genes) and IFN genes, which have been associated with tumor resistance to immunotherapies[19,20].

We first applied the 57-immune gene signature to a cohort of 98 human bladder cancer samples for which we also analyzed the mutational status of *PIK3CA, BRAF, RAS* and *FGFR3* genes, which are implicated in the activation of the respective oncogenic pathways (**Supplementary Figure 1)**. Using unsupervised hierarchical clustering, bladder cancers were segregated into “high” or “low” immune-infiltrated (also referred to as “hot” or “cold” tumors[17,21]) based on the level of expression of the immune gene signature. The high level of expression of the immune gene signature reflects the presence of a reactive immune infiltrate in the tumor microenvironment. Along these lines, we have previously confirmed that qRT-PCR mRNA and protein immunohistochemistry expression were strongly associated for immune markers in MIBC patients[22]. We observed that, as previously described[16], urothelial bladder cancers showed different levels of immune infiltration depending on the histological group type: NMIBCs showed a significantly lower expression of the immune gene signature than MIBCs (Fisher’s exact test, $p<0.001$). We also found that tumors bearing a *PIK3CA* mutation or a *FGFR3* mutation were significantly associated with a lower expression of the immune gene signature in comparison to their wild type counterparts (Fisher’s exact test, $p<0.05$ and $p<0.001$ respectively). *RAS*-mutated

tumors did not segregate into hot or cold tumors, and there was only one *BRAF* mutation found in this cohort of bladder tumor patients, in accordance with the low frequency of this oncogenic mutation in bladder tumors**.**

Given that NMIBCs showed very low levels of expression of the immune gene signature, we then focused on the MIBC subgroup. Among the 56 MIBC samples, we observed that tumors bearing a *PIK3CA* mutation showed a significantly lower expression of the immune gene signature compared to *PIK3CA*-unmutated ones (Fisher's exact test, p=0.04, **Figure 1A).** However, when we reduced the analysis to only MIBC samples, there were no significant associations between the expression of the immune gene signature and *FGFR3* mutational status (Fisher's exact test, not significant (NS)) or *RAS* mutational status (Fisher's exact test, NS, **Figure 1A**).

We then defined a minimal immune gene signature comprising the 10 most statistically significant differentially expressed genes between wild type and *PIK3CA*-mutated samples (according to Mann-Whitney Wilcoxon test), (**Figure 1B**). The 10 genes were *TIGIT, CTLA4, CD8A, GZMA, PVRIG, PDCD1, HAVCR2, ENTPD1, HLA-DRA, HLA-DRB*, which reflect an activated T-cell infiltrate in the tumor. Using this 10-gene signature, the *PIK3CA*-mutated tumors segregated from the *PIK3CA*-wild type tumors (p=0.02, Fisher exact test) and fell in the "cold" tumor cluster. Furthermore, this signature effectively discriminated high- versus low- immune-infiltrated MIBC tumors (p<0.0001, Fisher exact test).

Overall, our results suggest that mutations in the *PIK3CA* gene, leading to the activation of the PI3K pathway, are associated to a reduced immune infiltration of the tumor stroma of MIBCs.

Therapeutic inhibition of PI3K pathway inhibits tumor growth in a humanized mice model

To confirm the correlation between the *PIK3CA* gene activating mutation and the level of tumor T-cell-infiltrate in MIBCs, we set up a humanized mouse model allowing to directly assess the effect of a clinical-grade PI3K inhibitor on human tumor cells and human immune cells *in vivo*.

We used NOD scid gamma (NSG) recipient mice, which are highly immunodeficient, as they have no B, T and NK cells, and consequently allow the engraftment of tumor and immune cells of human origin[23,24]. Mice were subcutaneously injected with cells of either the VMCUB1 cell line, a *PIK3CA*-mutated human bladder cancer cell line, or as a control, the HT1376 cell line, a *PIK3CA*-wild type human bladder cancer cell line. When the tumors were palpable, mice were grafted with human peripheral blood mononuclear cells (PBMCs) isolated from blood samples of human healthy donors. In this humanized model, the majority of human immune cells that reconstitute the mice are T cells derived from the injected PBMCs[24]. Three days later, mice were assigned to: no treatment, or treatment with a class IA-PI3K inhibitor, BKM120 (**Figure 2A**). Individual and mean tumor growth curves of each cell line are shown in **Figures 2B and 2C,** respectively**.** In the *PIK3CA*-mutated VMCUB1 group, tumors in mice treated with BKM120 grew at a significantly slower rate, in comparison to the untreated mice (Mann-Whitney test, $P < 0.0005$, **Figures 2B and 2C**). In the *PIK3CA*-wild type HT1376 group, no significant effect of BKM120 on tumor growth was observed when compared to the untreated mice (**Figures 2B and 2C**).

The main caveat of this model is that the injected human PBMCs react against mice xeno-antigens, invariably leading to xeno-graft-versus-host-disease (GvHD), which

induces progressive body weight loss and death of the mice[24–26]. To evaluate GvHD development, we registered mice body weight along the length of the experiment. As shown in **Figure 2D,** no weight loss higher than 20% (what is considered as a hallmark of clinical GvHD) was observed until day 25 in any of the two models. Consequently, similar to the results already published using PBMC injection in NSG mice[24,27,28], the therapeutic observational window in this model is around 3-4 weeks after PBMCs injection, before evident signs of GvHD.

As BKM120 inhibited tumor growth, we used qRT-PCR to evaluate a panel of genes involved in cell cycling/division that could explain the direct drug effect on tumor cell proliferation. We assessed the expression profile of the proliferation genes *ETV4*, *ETV5*, *DUSP1*, which are downstream in the MAPK pathway, and the *CA9* gene which is downstream in the PI3K/AKT/mTOR pathway[29] (**Supplementary Figure 2**). These genes were significantly downregulated in the *PIK3CA*-mutated VMCUB1 humanized mice after BKM120 treatment, indicating an anti-proliferative effect and an efficient inhibition of the PI3K oncogenic pathway under BKM120 treatment. Although with this technique we cannot dissociate whether the anti-proliferative effect is occurring in the tumor or in other cells present in the microenvironment, the fact that the activating *PIK3CA* mutation is only present on the tumor cells suggests that variation on the proliferative genes is mainly occurring in the tumor. Altogether these data show that the class IA-PI3K inhibitor BKM120 significantly inhibited the growth of the *PIK3CA*-mutated VMCUB1 human bladder cancer cell line in a humanized mouse model.

Blocking PI3K signaling increases tumor-immune infiltrate

We then examined the changes that occurred in the intra-tumoral immune infiltrate upon inhibition of the PI3K pathway by BKM120. Total immune infiltration (HuCD45+ cells) was quantified by FACS in tumor samples harvested at sacrifice of mice at day 25 (**Figure 3A**). We observed that in the *PIK3CA*-mutated VMCUB1 group, BKM120 treatment significantly increased the proportion of HuCD45+ cells in the tumor ($p<0.001$), as well as the proportion of CD3+ T cells ($p<0.05$), in comparison to untreated mice. In tumors harvested from mice of the *PIK3CA*-wild type HT1376 group, there were no significant changes in the percentage of total immune cells or CD3+ T cells under BKM120 treatment. We then evaluated the distribution of different immune cell subpopulations in the tumor microenvironment. In the *PIK3CA*-mutated VMCUB1 group and in the *PIK3CA*-wild type HT1376 group, there were no statistically significant differences between the untreated and treated groups regarding the composition of immune T cells (including CD8+ cytotoxic, CD4+ FOXP3- conventional and CD4+ FOXP3+ regulatory T cells), B and NK cells (**Figure 3B**). Immunohistochemistry analysis of the tumor samples confirmed the presence of the transferred human hematopoietic cells in the tumor bed. Representative stainings are shown in **Figure 3C**, depicting the anatomic distribution of tumor-infiltrating huCD45+ cells, which were found not only at the periphery, but also interspaced among the tumor cells. Overall, these results suggest that at the dose used, BKM120 reduces the growth of *PIK3CA*-mutated tumors, yet it does not exert a sizeable toxic effect on T cells.

We further assessed the impact of BKM120 treatment on the immune gene expression profile using qRT-PCR analysis, of tumor samples from the humanized mouse model samples. **Supplementary Figure 3** shows the effect of BKM120 treatment on the expression of 19 evaluated immune genes (which we selected among the most

differentially expressed in **Figure 1A**). As it could be expected, we observed no or minimal expression of genes corresponding to human immune cell populations that are usually not found (or present at very low levels) in the tumor infiltrate of this humanized model, including neutrophils (*FUT4*), macrophages (*MERTK*), dendritic cells (*XCR1*), Tregs (*FOXP3*), NK cells (*NCAM1*) and B cells (*MS4A1*). **Figure 4** depicts individual mRNA expression of the genes that were statistically significantly modified by BKM120 treatment of VMCUB1 *PIK3CA*-mutated tumor-bearing mice, including *PTPRC* (HuCD45) ($p<0.005$), *CD3E* (CD3) ($p<0.005$), *CD8A* (CD8) ($p<0.05$) *GZMA* (granzyme A) ($p<0.005$), and *HLA-DRA* (HLA-DRA) ($p<0.05$). These genes were not significantly affected in the *PIK3CA*-wild type HT1376 samples. In *PIK3CA*-mutated VMCUB1 bearing humanized mice, we also observed a BKM120-mediated increase of the expression of immune checkpoint genes including *TIGIT* ($p<0.005$), *CTLA-4* ($p<0.05$), *PDCD1* (PD-1) ($P<0.005$), *HAVCR2* (TIM-3) ($p<0.0005$) and *ENTPD1* (CD39) ($p<0.0005$) (data not shown).

To gain insight into the mechanism underlying the efficacy of BKM120 on the control of *PIK3CA*-mutated VMCUB1 tumor growth, we used qRT-PCR to evaluate a panel of genes involved in leukocyte attraction and migration (that could explain the increased T-cell infiltration) (**Table 4**), including 36 genes coding for chemokines responsible for immune cell (effector or suppressive subsets) migration to the tumor, for molecules involved in angiogenesis and for several adhesion molecules. We compared the genes' expression level in untreated versus BKM120 treated mice. **Figure 5** shows those genes that were statistically differentially expressed upon treatment (**Figure 5A** shows fold-change expression, and **Figure 5B** and **Supplementary Figure 4** show quantification of individual genes). Transcripts up-regulated by BKM120 treatment

included *CXCL13* (known to recruit TFH cells)[30], *CCL2, CCL3, CCL5* (known to recruit monocytes and macrophages) and *CXCL9, CXCL10, CXCL11* (known to recruit CXCR3-expressing immune cells Th1, CD8+ T cells and NK cells)[31]. Transcripts down-regulated by BKM120 treatment included *ITGB3, ITGB5, ITGB8*, which code for adhesion molecules described to promote tumor invasion or tumor escape from immune control[32,33]. These results suggest that BKM120 treatment re-shapes the landscape of chemokines and integrins present in the tumor microenvironment, promoting tumor infiltration by immune cells.

Increased tumor-immune infiltration induced by PI3K-signaling blockade renders tumors sensitive to anti-PD-1

Recent studies indicate that sufficient tumor infiltration by T cells is essential for response to immunotherapy[12,18]. Consequently, increasing tumor-infiltrating T cells, as observed in BKM120 treatment of *PIK3CA*-mutated VMCUB1 tumors (**Figure 3 and Supplementary Figure 3)**, should improve the therapeutic efficacy of PD-1 checkpoint blockade therapy. To test this hypothesis, we evaluated the effect of combining BKM120 with an anti-PD-1 antibody used in the clinic (nivolumab) on tumor growth in the humanized mice (**Figure 6**). Mice bearing *PIK3CA*-mutated VMCUB1 tumors and grafted with human PBMCs were assigned to the following groups: untreated, BKM120 alone, nivolumab alone or the combination of both (**Figure 6A**). Individual curves and mean tumor growth curves are shown in **Figures 6B and 6C,** respectively. It can be observed that administration of nivolumab alone did not significantly affect tumor growth, BKM120 treatment alone significantly delayed tumor growth as previously observed in Figures 2B and 2C **(**One-way ANOVA and Kruskal-Wallis test $P< 0.01$**)**,

and both drugs combined showed an additional effect **(**One-way ANOVA and Kruskal-Wallis test *P*< 0.0001). We verified that no body weight loss higher than 20% (clinical definition of GvHD) occurred in any of the groups, during the first 25 days of the experiment (**Figure 6D**).

These results indicate that treatment of the *PIK3CA*-mutated VMCUB1 tumor with a targeted inhibitor rendered this PD-1 resistant tumor sensitive to immunotherapy, and therefore demonstrate the potential benefit of combining a targeted therapy with an immunotherapy.

To understand the requirement of immune cells for the observed synergistic effect of the combinatory treatment, we performed a similar experiment as in **Figure 6** in mice non-grafted with human PBMC (**Supplementary Figure 5).** We observed that BKM120 was efficient in inhibiting tumor growth even in the absence of human immune cells, but the additional effect of combining nivolumab with BKM120 strictly required the presence of human PBMCs, confirming that anti-PD-1 is acting through T cells.

Discussion

Sensitivity of tumors to therapies targeting immune checkpoints seems to be conditioned by the quality and quantity of the tumor immune infiltrate.

We defined a qRT-PCR-based immune gene signature that allows weighing in a semi-quantitative way the immune infiltrate of solid tumors and that could discriminate high T-cell infiltrated bladder tumors from low/non-T-cell infiltrated tumors. This signature, which can be reduced to 10 genes, represents a low-cost and rapid technique that could be adapted and further validated in the clinical setting to evaluate tumor immune infiltration, so as to help in the clinical management of cancer patients.

Moreover, our approach indicates that the combination of this signature with the mutational status of oncogenic genes represents a simple way to identify tumoral oncogenic pathways responsible for the exclusion of the immune infiltrate out of the tumor microenvironment. The identified druggable mutations could represent a potential target for combination with anti-checkpoint antibodies, allowing that T cells re-invigorated by the immunotherapy effectively access the tumor bed.

We found that in a cohort comprising 98 NMIBC and MIBC human samples, tumors bearing activating mutations in *PIK3CA* or *FGFR3* genes were associated with lower expression of the immune gene signature, compared to tumors bearing the wild-type genes, what could reflect the presence of a less active tumor immune infiltrate. Our findings confirm and extend a previous report associating FGFR3 pathway activation in non-T-cell-inflamed MIBCs, as well as a lower immune gene expression in NMIBCs compared to MIBCs[34]. When we focused on MIBC tumor sub-type, we observed that MIBCs from patients bearing *PIK3CA* gene mutations but not *BRAF, RAS* or *FGFR3* mutations were still significantly associated to non-T-cell-infiltrated tumors, compared to unmutated ones, which, to our knowledge, has not been reported before. These results indicate that the identified molecular events do not explain all the cases of infiltrated or non-infiltrated tumors. On the contrary, our work indicates that the influence of each oncogenic pathway on the immune infiltrate is tumor-type dependent and even more, tumor sub-type dependent, as was the case for the muscle-invasive and non-invasive bladder tumors in our studied series. Another point that could explain the fact that FGFR3 pathway was not associated to immune gene expression patterns in MIBC anymore is that *FGFR3* mutations are more frequent in NMIBC than MIBC[35].

To confirm this association between the tumor T-cell infiltrate in MIBCs and mutations of the *PIK3CA* gene, we set up a humanized mouse model allowing direct assessment

of the effect of a clinical-grade PI3K inhibitor on human tumor cells and human immune cells *in vivo*. We observed that BKM120, a pan class 1A-PI3K inhibitor, significantly inhibited the growth of a human bladder cancer cell line bearing a druggable *PIK3CA* mutation, associated with an increase in tumor infiltration by immune cell (HuCD45+) and more specifically CD3+ T cells.

Different primary and adaptive acquired mechanisms of resistance to immune checkpoint inhibitors have been described. Among them, the absence of tumor recognition by T cells, due to the lack of immunogenic tumor antigens (i.e. low mutational burden, absence of cancer-testis antigen), or to the development by the tumor of mechanisms that blunt antigen presentation (i.e. alterations in proteasome subunits or transporters associated with antigen processing or deletion of the beta-2-microblobulin or the MHC molecules themselves)[12,19,36]. Also, tumor-intrinsic activated oncogenic pathways have been associated with poor responses to immunotherapy. Along these lines, the loss of PTEN and consequent activation of the PI3K/AKT/mTOR pathway has been associated with a post-transcriptional increase of PD-L1 expression in gliomas[14], and to decreased T-cell infiltration at tumor sites in melanoma in part due to the increase in the expression of immunosuppressive cytokines[15]. Additionally, tumor-intrinsic active WNT/β-catenin signaling pathway has also been described to induce T-cell exclusion from the tumor tissue mediated by decreased production of chemokines[37]. Moreover, a panel of chemokines (CCL2, CCL3, CCL4, CCL5, CXCL9 and CXCL10) was described to be expressed in metastatic melanomas rich in infiltrating T-cells[8]. These results are in accordance with the upregulated chemokine transcripts that we detected after inhibition of the PI3K pathway. Furthermore, we observed that adhesion molecules' expression (ITGB3, ITGB5 and ITGB8) was

downregulated after BKM120 administration, which could further contribute to the increase in tumor infiltration by immune cells, as previously described[33,38]).

The anti-tumoral immune response can also be inhibited by immunosuppressive cells, such as Tregs and tumor-associated macrophages. Indeed, inhibition of PI3K pathway could also have an inhibitory effect on myeloid-derived suppressor cells (MSDCs), which could restore the activity of T cells, without increasing the quantity of T cells present in the tumor micro-environment, but leading to an increase of activated T cells. This has been shown for anti-angiogenic treatments which seem to act, at least in part, by reducing the number of MSDCs in tumor immune infiltrate, and consequently promoting the activation of T cells. This hypothesis has been investigated recently in a head and neck squamous cell carcinoma model, in which inhibition of PI3K pathway with a PI3K inhibitor could functionally inhibit MDSCs, leading to enhanced responses to PD-L1 blockade. Moreover, in this model, combination therapy of this PI3K inhibitor with anti-PD-L1 antibody induced CD8+ T cell dependent primary tumor growth delay[39]. However, in the humanized mouse model that we used for our study, the human myeloid cells do not efficiently reconstitute the immunodeficient mice, hampering the evaluation of the therapy's effect on human myeloid cells.

Finally, we observed that inhibition of the PI3K pathway effectively increased immune infiltration of *PIK3CA*-mutated bladder tumors, thus transforming "cold" tumors into "hot" tumors, which is thought to represent a key step in obtaining significant responses to immunotherapies. We describe that BKM120 induced an increase of the expression of several immune cell population genes such as *PTPRC* (HuCD45), *CD3E* (CD3), *CD8A* (CD8) or *GZMA* (granzyme A) reflecting an increasing active immune infiltrate, along with genes encoding for immune checkpoints such as TIGIT, CTLA-4, PD-1, TIM-3, or CD39, suggesting potential for tumor sensitivity to immune checkpoint

blockade, and identifying other potential immune checkpoint targets other than anti-CTLA-4 and anti-PD-1/PD-L1 antibodies. Furthermore, our data showed that the combination of a PI3K inhibitor and nivolumab treatment rendered an anti-PD-1 resistant tumor sensitive to the immunotherapy.

Our results suggest a relevant rationale for combination strategies of PI3K inhibitors with immune checkpoint inhibitors. Actually, several combination strategies of immune checkpoint inhibitors with either molecularly targeted therapies, chemotherapy, radiotherapy, or other immunotherapies in development are evaluated, to try to overcome primary resistance to immune checkpoint inhibitors in various tumor types[40]. Strategies evaluating PI3K inhibitors in combination with immune checkpoint inhibitors are already being assessed in early clinical trials[41].

Further studies will be needed to better decipher the mechanisms of immune resistance, and also to define the most efficient combination strategies, with the most efficient timing and dosage of targeted and immune therapies.

Materials and Methods

Classification of urothelial bladder cancer subtypes by immune gene expression profile and presence of mutations in oncogenic pathways

Patients and samples

Patients included 17 women (17.3%) and 81 men (82.7%). Pathological staging included 42 NMIBC, 18 low-grade (42.9%) and 24 high-grade (57.1%) NMIBC, and 56

high-grade MIBC. Clinical and histological characteristics of patients along with survival are summarized in **Tables 2 and 3.**

Patients included in this study had undergone transurethral bladder resection or radical cystectomy in Cochin hospital between January 2002 and January 2006. Data were obtained from patient's medical records. All patients signed an informed consent. This study received approval from an institutional review board and was conducted according to the principles outlined in the Declaration of Helsinki.

Immediately after surgery, tumor samples were frozen in liquid nitrogen and stored at -80°C (for RNA extraction) and fixed in formaldehyde.

qRT-PCR analysis of the immune gene signature in human bladder tumor samples

The theoretical basis, RNA extraction, cDNA synthesis, design of primers and PCR reaction conditions have been previously described in detail[42]. Briefly, quantitative values were obtained from the threshold cycle (Ct) number at which the increase in the signal associated with the exponential growth of PCR products began to be detected. One endogenous RNA control gene was chosen, namely *TB*P (Gen-Bank Accession No.NM_003194), which encodes TATA box-binding protein. Each sample was normalized based on its *TBP* content. Results, expressed as N-fold differences in target gene expression relative to the *TBP* gene and termed N*target*, were determined as N*target* = $2^{Ct\ sample}$, where the Ct value of the sample was determined by subtracting the average Ct value of the target gene from the average Ct value of the TBP gene. For all genes, a Ct value below 38 was considered as quantifiable and the mRNA values were normalized such that a Ct value of 38 was equal to 0.125, i.e. smallest quantifiable amount of mRNA. A Ct value above 38 was considered as not quantifiable. Positive controls for all genes were obtained by performing an RNA pool control, which

was prepared by mixing identical amounts of RNA from various human normal and tumoral tissues.

To generate the heatmaps we used the “heatmap.3 function in the R software”. Hierarchical clusterings were produced using as input the log2 expression values of normalized Ct, using Ward’s method on euclidean distances. To solve the error caused by log transformation of values of 0, we have added 0.001 to all values before log transformation. Values in the heatmap are expressed as log2 (normalized Ct), where (as explained above), a normalized Ct value of 38 is equal to 0.125 (then, log2(0.125)= -3). This means that in the heatmap all values lower than -3 correspond to non-quantifiable expression of a gene. Fisher’s exact test was applied to verify if identified clusterings permit to discriminate wild type and mutated samples for each oncogenic pathway according to the immune gene signature.

Mann-Whitney-Wilcoxon test was applied between wild type and mutated gene sample populations on each gene to identify the genes that were statistically differentially expressed between both populations.

Evaluation of the effect of targeted therapy inhibition of PI3K pathway on tumor-immune infiltration in vivo

Humanized mouse model

NOD-*scid*-IL2rγ-/- (NSG) mice were grafted with human tumor cell line and then reconstituted with human peripheral blood mononuclear cells (PBMC) from blood samples of healthy donors.

PBMC were isolated using Ficoll and the quantification of CD3+ cells was done by Fluorescence-activated cell sorting (FACS) and then the total PBMC were immediately stored in liquid nitrogen.

Human bladder cancer cell lines, either VMCUB1, a *PIK3CA*-mutated human bladder cell line, or HT1376, a *PIK3CA*-wild type human bladder cancer cell line, were injected ectopically in the right flank of each NSG mouse subcutaneously with 10 or 20 x 10^6 of cancer cells/mouse.

When the tumors were palpable (above 3x3mm), we injected intravenously (IV), by retro orbital injection, the amount of PBMC that corresponds to 7.5 x 10^6 human CD3+ T cells/mouse.

Tumor growth was measured twice a week using a caliper to determine the tumor size, calculated as ((length x $width^2$)/2). Mice were sacrificed before the tumor reached 2 cm^3. Mice were weighted at the same time points, to follow graft versus host disease (GvHD), and following ethical guidance, were sacrificed upon a loss of 20% of body weight, considered as clinical diagnosis of GvHD.

Starting 3 days after PBMC injection, BKM120 (MedChemExpress), a pan-PI3K inhibitor, was administered at a dose of 30 mg/kg per day, via oral gavage every day. Nivolumab (OPDIVO, BMS) is also administered (i.p.) 3 days after PBMC injection at a dose of 10mg/kg twice a week.

At the experimental endpoint, mice were sacrificed; the tumors were collected and processed individually. Half of each tumor sample was used for FACS staining and the other half was divided in two, one part was used for the histochemistry analysis, and the other was kept in liquid nitrogen directly after dissection for future qPCR analysis to assess our immune gene signature on tumor samples from the humanized mouse model.

Flow cytometry

Half of the tumor was processed for FACS analysis. The tumor was cut into small pieces and mixed with 2ml of CO2 independent medium (Gibco® Life technologie) containing 30 µl Dnase (10mg/ml, Roche®), and 60 µl liberase LT (5mg/ml, Roche®) per sample. The tumor sample was processed on a Gentlemacs dissociator (Miltenyi Biotec, San Diego, CA) according to the manufacturer's instructions, then the dissociated tumor sample was filtered through a cell strainer (BD Biosciences), washed with PBS, then incubated with the antibodies (Abs) for FACS staining.

For the phenotypic analysis of human immune cell populations, tumor cells were stained for surface markers with LIVE/DEAD Fixable Aqua (Life TechnologiesTM), hCD27-BV605 clone O323 (Biolegend), hCD3-BV650 clone OKT3 (Biolegend), hCD4-BV785 clone OKT4 (Biolegend), hPD-1-BV711 clone EH12.2H7 (Biolegend), hCD8-PECF594 clone RPA-T8 (BD Biosciences), hCD56-PE-Cy5 clone N901 (BD Biosciences), hCD45-APC Cy7 clone 2D1 (BD Biosciences), hCD19-Alexa 700 clone HIB19 (BD Biosciences), hCD45RA-PECy5 clone HI100 (eBiosciences), hCD25-PE (BD Biosciences), hTCRgd-FITC clone 11F2 (BD Biosciences). Then for intracellular staining, cells were fixed and permeabilized with fixation/permeabilization solution (eBiosciences) according to the manufacturer's instructions and stained with FOXP3-efluor 450 clone 236A/E7, (eBioscience).

Samples were then analyzed on a Fortessa flow cytometer (BD Biosciences). FACS data were analyzed with FlowJo Version v10.0.8 (TreeStar).

Immunohistochemistry

Paraffin-embedded tumors from mice untreated or treated with BKM120 were stained for human CD45 cells. Sequential sections of 3μm were cut, deparaffinized and rehydrated through a series of xylene and ethanol washes. The samples were then exposed to citrate buffer pH 6 (Dako) for 20 minutes in a microwave (antigen retrieval) followed by an incubation of 10 minutes with 3% hydrogen peroxidase in deionized water (blocking of endogenous peroxidase), and washed with water and PBS. The samples were then incubated with anti-human CD45 Ab (2B11 and PD7/26 clones, Dako) followed by immunodetection with the biotin-conjugated anti-mouse antibody. Afterwards, the samples were incubated with peroxidase-labeled streptavidin and followed by chromogenic reaction with DAB counterstaining with hematoxylin. All the staining process was performed using a Dako autostainer.

Authors' Contributions:

B.E., DLR. P. B. I. and. P. E. designed the research. B.E., DLR. P., V.S., D. M., C. S. and C.W. performed experiments and analyzed data. R.A. R.W. performed bioinformatic analysis. K.C., R.F. and Y.A. provided reagents and contributed to experimental design. P.G., B.L. and D.D contributed with patient data and samples, B. I., A. Y; R.F and P. E. critically revised the manuscript. B.E., DLR. P. and. P.E. wrote the manuscript. P.E. conceived and designed the project and wrote the manuscript.

Acknowledgements:

We thank the mouse facility, flow cytometry core, and the Pathex platform from Institut Curie. This work was supported by the Institut Curie, Institut National de la Santé et de la Recherche Médicale, Association pour la Recherche sur le Cancer (ARC PJA 20131200444); Labex DCBIOL (ANR-10-IDEX-0001-02 PSL and ANR-11-

LABX0043), SIRIC INCa-DGOS-Inserm_12554. B.E. was supported by a master 2 fellowship from Institut Curie.

Conflicts of interest: The authors declare no competing financial interests.

References

1. Torre LA, Bray F, Siegel RL, Ferlay J, Lortet-Tieulent J, Jemal A. Global cancer statistics, 2012. CA Cancer J Clin. 2015;65(2):87–108. doi:10.3322/caac.21262

2. Sylvester RJ, van der Meijden APM, Oosterlinck W, Witjes JA, Bouffioux C, Denis L, Newling DWW, Kurth K. Predicting recurrence and progression in individual patients with stage Ta T1 bladder cancer using EORTC risk tables: a combined analysis of 2596 patients from seven EORTC trials. Eur. Urol. 2006;49(3):466–465; discussion 475-477. doi:10.1016/j.eururo.2005.12.031

3. von der Maase H, Hansen SW, Roberts JT, Dogliotti L, Oliver T, Moore MJ, Bodrogi I, Albers P, Knuth A, Lippert CM, et al. Gemcitabine and cisplatin versus methotrexate, vinblastine, doxorubicin, and cisplatin in advanced or metastatic bladder cancer: results of a large, randomized, multinational, multicenter, phase III study. J. Clin. Oncol. 2000;18(17):3068–3077. doi:10.1200/JCO.2000.18.17.3068

4. Bellmunt J, Fougeray R, Rosenberg JE, von der Maase H, Schutz FA, Salhi Y, Culine S, Choueiri TK. Long-term survival results of a randomized phase III trial of vinflunine plus best supportive care versus best supportive care alone in advanced urothelial carcinoma patients after failure of platinum-based chemotherapy. Ann. Oncol. 2013;24(6):1466–1472. doi:10.1093/annonc/mdt007

5. Rosenberg JE, Hoffman-Censits J, Powles T, van der Heijden MS, Balar AV, Necchi

A, Dawson N, O'Donnell PH, Balmanoukian A, Loriot Y, et al. Atezolizumab in patients with locally advanced and metastatic urothelial carcinoma who have progressed following treatment with platinum-based chemotherapy: a single-arm, multicentre, phase 2 trial. Lancet. 2016;387(10031):1909–1920. doi:10.1016/S0140-6736(16)00561-4

6. Bellmunt J, de Wit R, Vaughn DJ, Fradet Y, Lee J-L, Fong L, Vogelzang NJ, Climent MA, Petrylak DP, Choueiri TK, et al. Pembrolizumab as Second-Line Therapy for Advanced Urothelial Carcinoma. N. Engl. J. Med. 2017;376(11):1015–1026. doi:10.1056/NEJMoa1613683

7. Topalian SL, Hodi FS, Brahmer JR, Gettinger SN, Smith DC, McDermott DF, Powderly JD, Carvajal RD, Sosman JA, Atkins MB, et al. Safety, activity, and immune correlates of anti-PD-1 antibody in cancer. N. Engl. J. Med. 2012;366(26):2443–2454. doi:10.1056/NEJMoa1200690

8. Harlin H, Meng Y, Peterson AC, Zha Y, Tretiakova M, Slingluff C, McKee M, Gajewski TF. Chemokine expression in melanoma metastases associated with CD8+ T-cell recruitment. Cancer Res. 2009;69(7):3077–3085. doi:10.1158/0008-5472.CAN-08-2281

9. Ji R-R, Chasalow SD, Wang L, Hamid O, Schmidt H, Cogswell J, Alaparthy S, Berman D, Jure-Kunkel M, Siemers NO, et al. An immune-active tumor microenvironment favors clinical response to ipilimumab. Cancer Immunol. Immunother. 2012;61(7):1019–1031. doi:10.1007/s00262-011-1172-6

10. Kirilovsky A, Marliot F, El Sissy C, Haicheur N, Galon J, Pagès F. Rational bases for the use of the Immunoscore in routine clinical settings as a prognostic and predictive biomarker in cancer patients. Int. Immunol. 2016;28(8):373–382. doi:10.1093/intimm/dxw021

11. Pagès F, Berger A, Camus M, Sanchez-Cabo F, Costes A, Molidor R, Mlecnik B, Kirilovsky A, Nilsson M, Damotte D, et al. Effector memory T cells, early metastasis, and survival in colorectal cancer. N. Engl. J. Med. 2005;353(25):2654–2666. doi:10.1056/NEJMoa051424

12. Ramos RN, Piaggio E, Romano E. Mechanisms of Resistance to Immune Checkpoint Antibodies. Handb Exp Pharmacol. 2017 Mar 18. doi:10.1007/164_2017_11

13. Yuan TL, Cantley LC. PI3K pathway alterations in cancer: variations on a theme. Oncogene. 2008;27(41):5497–5510. doi:10.1038/onc.2008.245

14. Parsa AT, Waldron JS, Panner A, Crane CA, Parney IF, Barry JJ, Cachola KE, Murray JC, Tihan T, Jensen MC, et al. Loss of tumor suppressor PTEN function increases B7-H1 expression and immunoresistance in glioma. Nat. Med. 2007;13(1):84–88. doi:10.1038/nm1517

15. Peng W, Chen JQ, Liu C, Malu S, Creasy C, Tetzlaff MT, Xu C, McKenzie JA, Zhang C, Liang X, et al. Loss of PTEN Promotes Resistance to T Cell-Mediated Immunotherapy. Cancer Discov. 2016;6(2):202–216. doi:10.1158/2159-8290.CD-15-0283

16. Sweis RF, Spranger S, Bao R, Paner GP, Stadler WM, Steinberg G, Gajewski TF. Molecular Drivers of the Non-T-cell-Inflamed Tumor Microenvironment in Urothelial Bladder Cancer. Cancer Immunol Res. 2016;4(7):563–568. doi:10.1158/2326-6066.CIR-15-0274

17. Chen DS, Mellman I. Elements of cancer immunity and the cancer-immune set point. Nature. 2017;541(7637):321–330. doi:10.1038/nature21349

18. Galon J, Bruni D. Approaches to treat immune hot, altered and cold tumours with combination immunotherapies. Nat Rev Drug Discov. 2019 Jan 4.

doi:10.1038/s41573-018-0007-y

19. Sucker A, Zhao F, Real B, Heeke C, Bielefeld N, Maβen S, Horn S, Moll I, Maltaner R, Horn PA, et al. Genetic evolution of T-cell resistance in the course of melanoma progression. Clin. Cancer Res. 2014;20(24):6593–6604. doi:10.1158/1078-0432.CCR-14-0567

20. Gao J, Shi LZ, Zhao H, Chen J, Xiong L, He Q, Chen T, Roszik J, Bernatchez C, Woodman SE, et al. Loss of IFN-γ Pathway Genes in Tumor Cells as a Mechanism of Resistance to Anti-CTLA-4 Therapy. Cell. 2016;167(2):397-404.e9. doi:10.1016/j.cell.2016.08.069

21. Spranger S, Spaapen RM, Zha Y, Williams J, Meng Y, Ha TT, Gajewski TF. Up-Regulation of PD-L1, IDO, and Tregs in the Melanoma Tumor Microenvironment Is Driven by CD8+ T Cells. Science Translational Medicine. 2013;5(200):200ra116-200ra116. doi:10.1126/scitranslmed.3006504

22. Le Goux C, Vacher S, Pignot G, Sibony M, Barry Delongchamps N, Terris B, Piaggio E, Zerbib M, Damotte D, Bieche I. mRNA Expression levels of genes involved in antitumor immunity: Identification of a 3-gene signature associated with prognosis of muscle-invasive bladder cancer. Oncoimmunology. 2017;6(11):e1358330. doi:10.1080/2162402X.2017.1358330

23. Shultz LD, Ishikawa F, Greiner DL. Humanized mice in translational biomedical research. Nat. Rev. Immunol. 2007;7(2):118–130. doi:10.1038/nri2017

24. De La Rochere P, Guil-Luna S, Decaudin D, Azar G, Sidhu SS, Piaggio E. Humanized Mice for the Study of Immuno-Oncology. Trends Immunol. 2018;39(9):748–763. doi:10.1016/j.it.2018.07.001

25. Pérol L, Martin GH, Maury S, Cohen JL, Piaggio E. Potential limitations of IL-2 administration for the treatment of experimental acute graft-versus-host disease.

Immunol. Lett. 2014;162(2 Pt B):173–184. doi:10.1016/j.imlet.2014.10.027

26. Naserian S, Leclerc M, Thiolat A, Pilon C, Le Bret C, Belkacemi Y, Maury S, Charlotte F, Cohen JL. Simple, Reproducible, and Efficient Clinical Grading System for Murine Models of Acute Graft-versus-Host Disease. Front Immunol. 2018;9:10. doi:10.3389/fimmu.2018.00010

27. Ito M, Hiramatsu H, Kobayashi K, Suzue K, Kawahata M, Hioki K, Ueyama Y, Koyanagi Y, Sugamura K, Tsuji K, et al. NOD/SCID/gamma(c)(null) mouse: an excellent recipient mouse model for engraftment of human cells. Blood. 2002;100(9):3175–3182. doi:10.1182/blood-2001-12-0207

28. King MA, Covassin L, Brehm MA, Racki W, Pearson T, Leif J, Laning J, Fodor W, Foreman O, Burzenski L, et al. Human peripheral blood leucocyte non-obese diabetic-severe combined immunodeficiency interleukin-2 receptor gamma chain gene mouse model of xenogeneic graft-versus-host-like disease and the role of host major histocompatibility complex. Clin. Exp. Immunol. 2009;157(1):104–118. doi:10.1111/j.1365-2249.2009.03933.x

29. Burgess MR, Hwang E, Mroue R, Bielski CM, Wandler AM, Huang BJ, Firestone AJ, Young A, Lacap JA, Crocker L, et al. KRAS Allelic Imbalance Enhances Fitness and Modulates MAP Kinase Dependence in Cancer. Cell. 2017;168(5):817-829.e15. doi:10.1016/j.cell.2017.01.020

30. de Leval L, Rickman DS, Thielen C, Reynies A de, Huang Y-L, Delsol G, Lamant L, Leroy K, Brière J, Molina T, et al. The gene expression profile of nodal peripheral T-cell lymphoma demonstrates a molecular link between angioimmunoblastic T-cell lymphoma (AITL) and follicular helper T (TFH) cells. Blood. 2007;109(11):4952–4963. doi:10.1182/blood-2006-10-055145

31. Nagarsheth N, Wicha MS, Zou W. Chemokines in the cancer microenvironment

and their relevance in cancer immunotherapy. Nat. Rev. Immunol. 2017;17(9):559–572. doi:10.1038/nri.2017.49

32. Sloan EK, Pouliot N, Stanley KL, Chia J, Moseley JM, Hards DK, Anderson RL. Tumor-specific expression of alphavbeta3 integrin promotes spontaneous metastasis of breast cancer to bone. Breast Cancer Res. 2006;8(2):R20. doi:10.1186/bcr1398

33. Takasaka N, Seed RI, Cormier A, Bondesson AJ, Lou J, Elattma A, Ito S, Yanagisawa H, Hashimoto M, Ma R, et al. Integrin αvβ8-expressing tumor cells evade host immunity by regulating TGF-β activation in immune cells. JCI Insight. 2018;3(20). doi:10.1172/jci.insight.122591

34. Sweis RF, Spranger S, Bao R, Paner GP, Stadler WM, Steinberg G, Gajewski TF. Molecular Drivers of the Non-T-cell-Inflamed Tumor Microenvironment in Urothelial Bladder Cancer. Cancer Immunol Res. 2016;4(7):563–568. doi:10.1158/2326-6066.CIR-15-0274

35. Kompier LC, Lurkin I, van der Aa MNM, van Rhijn BWG, van der Kwast TH, Zwarthoff EC. FGFR3, HRAS, KRAS, NRAS and PIK3CA mutations in bladder cancer and their potential as biomarkers for surveillance and therapy. PLoS ONE. 2010;5(11):e13821. doi:10.1371/journal.pone.0013821

36. Sharma P, Hu-Lieskovan S, Wargo JA, Ribas A. Primary, Adaptive, and Acquired Resistance to Cancer Immunotherapy. Cell. 2017;168(4):707–723. doi:10.1016/j.cell.2017.01.017

37. Spranger S, Bao R, Gajewski TF. Melanoma-intrinsic β-catenin signalling prevents anti-tumour immunity. Nature. 2015;523(7559):231–235. doi:10.1038/nature14404

38. Chae YK, Choi WM, Bae WH, Anker J, Davis AA, Agte S, Iams WT, Cruz M, Matsangou M, Giles FJ. Overexpression of adhesion molecules and barrier molecules is associated with differential infiltration of immune cells in non-small cell lung cancer.

Sci Rep. 2018;8(1):1023. doi:10.1038/s41598-018-19454-3

39. Davis RJ, Moore EC, Clavijo PE, Friedman J, Cash H, Chen Z, Silvin C, Van Waes C, Allen C. Anti-PD-L1 Efficacy Can Be Enhanced by Inhibition of Myeloid-Derived Suppressor Cells with a Selective Inhibitor of PI3Kδ/γ. Cancer Res. 2017;77(10):2607–2619. doi:10.1158/0008-5472.CAN-16-2534

40. Vanneman M, Dranoff G. Combining Immunotherapy and Targeted Therapies in Cancer Treatment. Nat Rev Cancer. 2012;12(4):237–251. doi:10.1038/nrc3237

41. Sullivan RJ, Hong D, Tolcher A, Patnaik A, Shapiro G, Chmielowski B. Initial results from first-in-human study of IPI-549, a tumor macrophage-targeting agent, combined with nivolumab in advanced solid tumors. J Clin Oncol 2018; 36 (suppl; abstr 3013).

42. Bièche I, Onody P, Tozlu S, Driouch K, Vidaud M, Lidereau R. Prognostic value of ERBB family mRNA expression in breast carcinomas. Int. J. Cancer. 2003;106(5):758–765. doi:10.1002/ijc.11273

Figure legends

Figure 1: Heatmaps displaying unsupervised clustering of MIBCs into "high" or "low" immune-infiltrated tumors based on immune gene expression and displaying *PIK3CA* mutational status.

A. Hierarchical clustering heatmap of 56 MIBCs according to the qRT-PCR expression level of 57 immune genes. Dotted line delimitates clusters of "high" or "low" immune-infiltrated tumors, based on the level of expression of immune genes. Presence or

absence of activating mutations of *PIK3CA, BRAF, RAS and FGFR3* oncogenes is indicated, along with tumor stage and tumor grade for each sample. MIBCs bearing a *PIK3CA* mutation show a significantly lower expression of the immune gene signature than wild type tumors (Fisher's exact test, $p<0.05$). Gradient represents the log2 C_T value for each gene (yellow = high expression, blue-violet = low expression, dark blue = no expression).

B. Hierarchical clustering heatmap of 56 MIBCs according to the qRT-PCR expression level of the 10 most statistically significant differentially expressed genes between wild type and *PIK3CA*-mutated samples (according to Mann-Whitney Wilcoxon test). Dotted line delimitates clusters of "high" or "low" immune-infiltrated tumors, based on the level of expression of immune genes. *PIK3CA*-mutated tumors segregate from the *PIK3CA*-wild type tumors ($p<0.05$, Fisher exact test) and fall in the "low" immune-infiltrated tumor cluster. Gradient represents the log2 C_T value for each gene (yellow = high expression, blue-violet = low expression, dark blue = no expression).

Figure 2: Effect of BKM120 treatment on the growth of VMCUB1, *PIK3CA*-mutated and HT1376, *PIK3CA*-wild type human bladder tumors in humanized mice.

A. Experimental protocol: NSG mice were s.c. grafted with the indicated tumor cell line, and when tumors were palpable, they were i.v. injected with PBMCs. Three days later, mice were randomized to the "untreated" (N=14) or "BKM120-treated" (N=14) groups. BKM120 was administered daily at a dose of 30mg/kg by oral gavage.

B-C. Growth kinetics (**B**: individual curves; **C**: mean curves + standard error of the mean) of VMCUB1 (left panel) and HT1376 (right panel) tumors; untreated (black lines), BKM120-treated (blue lines). Tumors were measured twice per week.

D. GvHD was followed by the loss of body weight, shown as a percentage of initial weight (mean curves).

Results shown are the pool of two independent experiments with similar results. Statistical significance was calculated using the Mann-Whitney test. NS, not significant; ***, $P < 0.0005$.

Figure 3: Effect of BKM120 treatment on the tumor immune infiltrate of VMCUB1, *PIK3CA*-mutated and HT1376, *PIK3CA*-wild type human bladder tumors in humanized mice.

Humanized mice were treated as in Figure 2 and tumors were analyzed at day 25.

A. FACS analysis showing the proportion of total HuCD45+ and CD3+ T cells infiltrating the tumor, among live cells. Left panels: *PIK3CA*-mutated VMCUB1 tumors (N=8 in each group); right panels: *PIK3CA*-wild type HT1376 tumors (N=6 in the untreated group and N=7 in the BKM120 group).

B. Proportion of the indicated immune cell subsets among tumor-infiltrating HuCD45+ cells.

Results shown are from one representative experiment out of two with similar results. Statistical significance was calculated using the Mann-Whitney test. NS, not significant; *, $P < 0.05$; **, $P < 0.01$.

C. VMCUB1 *PIK3CA*-mutated tumors from untreated and BKM120-treated mice were characterized by IHC for human infiltrate (HuCD45). Representative IHC stainings of

two mice per indicated group are shown with two different magnifications: smaller square, x50; larger square, x400.

Figure 4: Immune gene expression changes induced by BKM120 treatment on *PIK3CA*-mutated VMCUB1 and *PIK3CA*-wild type HT1376 human bladder tumors in humanized mice.

NSG humanized mice were treated with BKM120 or untreated, as detailed in **Figure 2** and tumors were analyzed at day 25. Shown is the mRNA expression quantified by qRT-PCR of the indicated genes in *PIK3CA*-mutated VMCUB1 tumors (left panels) and *PIK3CA*-wild type HT1376 tumors (right panels), untreated (black dots) or BKM120-treated (blue dots). *PIK3CA*-mutated VMCUB1 tumors: N=13 in the untreated group and N=15 in the BKM120 group. *PIK3CA*-wild type HT1376 tumors: N=12 in the untreated group and N=13 in the BKM120 group. Statistical significance was calculated using the Mann-Whitney test; * $p<0.05$, ** $p<0.01$.

Figure 5: Chemokines and adhesion molecules gene expression changes induced by BKM120 treatment on *PIK3CA*-mutated VMCUB1 human bladder tumors in humanized mice.

NSG humanized mice grafted with VMCUB1 *PIK3CA*-mutated tumors were treated with BKM120 or untreated, as detailed in **Figure 2** and tumors were analyzed at day 25. mRNA expression of selected chemokines and adhesion molecules was quantified by qRT-PCR. **A.** Waterfall plot displaying fold-change expression, between BKM120-treated versus non-treated samples, of genes showing a significant statistical difference among 36 genes tested. The genes upregulated in BKM120-treated tumors are in yellow and the genes downregulated are in blue. **B.** Shown is the mRNA

expression of indicated genes (shown in A) for individual mice (**see also Supplementary Figure 4**). N=8 per group. Statistical significance was calculated using the Mann-Whitney test; * p<0.05, ** p<0.01, *** p<0.0005.

Figure 6: Nivolumab synergizes with BKM120 to reduce the growth of VMCUB1, *PIK3CA*-mutated human bladder tumors in humanized mice.

A. Experimental protocol: NSG mice were s.c. grafted with VMCUB1, *PIK3CA*-mutated tumor cells, and when tumors were palpable, they were i.v. injected with PBMCs. Three days later, mice were randomized to the "untreated" (N=23), "BKM120-treated" (N=23), "nivolumab-treated" (N=16) or combined "nivolumab-plus-BKM120-treated" (N=16) groups. BKM120 was administered daily at a dose of 30mg/kg by oral gavage and nivolumab was administered two times per week at a dose of 10mg/kg, i.p.

B-C. Tumor growth kinetics (**B**: individual curves; **C**: mean curves + standard error of the mean) of VMCUB1, *PIK3CA*-mutated tumors untreated (black line), treated with nivolumab (red line), BKM120 (blue line) or combination of both (green line). Tumors were measured twice per week.

D. GvHD was followed by the loss of body weight shown as a percentage of initial weight (mean curves). Results shown are the pool of three independent experiments with similar results. Statistical significance was calculated using One-way ANOVA and Kruskal-Wallis test. **, $P< 0.01$, ****, $P< 0.0001$.

Supplementary Figure 1: Heatmap displaying unsupervised clustering of bladder tumors into "high" or "low" immune-infiltrated tumors based on immune gene expression.

Hierarchical clustering heatmap of 98 human bladder cancer samples according to the qRT-PCR expression level of 57 immune genes. Dot-line delimitates clusters of “high” or “low” immune-infiltrated tumors, based on the level of expression of immune genes. NMIBCs show a significantly lower expression of the immune gene signature than MIBCs (Fisher’s exact test, $p<0.001$). Gradient represents the log2 C_T value for each gene (yellow = high expression, blue-violet = low expression, dark blue = no expression).

Supplementary Figure 2: BKM120 treatment effect on the expression of proliferation genes in *PIK3CA*-mutated VMCUB1 and *PIK3CA*-wild type HT1376 human bladder cancer cell line in a humanized mouse model.

Mice were treated as in **Figure 2** and tumors were analyzed at day 25. mRNA expression of the indicated genes quantified by qRT-PCR in *PIK3CA*-mutated VMCUB1 tumors (left panels) and *PIK3CA*-wild type HT1376 tumors (right panels), untreated (black dots) or BKM120-treated (blue dots). Statistical significance was calculated using the Mann-Whitney test; *** $p<0.0005$, **** $p<0.0001$.

Supplementary Figure 3: Heatmap displaying immune gene expression changes induced by BKM120 treatment on *PIK3CA*-mutated VMCUB1 and *PIK3CA*-wild type HT1376 human bladder tumors in humanized mice.

Mice were treated as in Figure 2 and tumors were analyzed at day 25. Heatmap shows the qRT-PCR expression level of 19 selected immune genes. Gradient represents the log2 C_T value for each gene (yellow = high expression, blue-violet = low expression, dark blue = no expression).

Supplementary Figure 4: Adhesion molecules gene expression changes induced by BKM120 treatment on *PIK3CA*-mutated VMCUB1 human bladder tumors in humanized mice.

Mice were treated as in **Figure 2** and tumors were analyzed at day 25. The mRNA expression of selected adhesion molecules was quantified using qRT-PCR. Shown is the mRNA expression of indicated genes for individual mice, N=8 per group. Statistical significance was calculated using the Mann-Whitney test; ** $p<0.01$, *** $p<0.0005$.

Supplementary Figure 5: Nivolumab/BKM120 combination requires human PBMC to be effective on VMCUB1, *PIK3CA*-mutated human bladder tumor.

The experiment was performed as described in **Figure 6**, except that *PIK3CA*-mutated VMCUB1 tumor-bearing mice did not receive PBMCs. In more detail, NSG mice were s.c. grafted with VMCUB1, *PIK3CA*-mutated tumor cells, and three days after tumors became palpable, mice were randomized to the “untreated” (black line), “BKM120-treated” (blue line), “nivolumab-treated” (red line), or combined “nivolumab-plus-BKM120-treated” (green line) groups, (N=7 to 8 mice per group). Shown are tumor growth kinetics (mean curves + standard error of the mean). Tumors were measured twice per week.

Tables

Table 1: List of the 57 genes selected for the immune gene signature

ID	GeneID	GeneSymbol	GeneName
Immune cell population genes			
CD2	914	CD2	CD2 molecule
CD3E	916	CD3E	CD3e molecule
CD4	920	CD4	CD4 molecule
CD8A	925	CD8A	CD8a molecule

CTLA4	1493	CTLA4	cytotoxic T-lymphocyte associated protein 4
FOXP3	50943	FOXP3	forkhead box P3
XCR1	2829	XCR1	chemokine (C motif) receptor 1
MERTK	10461	MERTK	MER proto-oncogene, tyrosine kinase
PTPRC	5788	PTPRC CD45	protein tyrosine phosphatase, receptor type C
MS4A1	931	MS4A1 CD20	membrane spanning 4-domains A1
NCAM1	4684	NCAM1 CD56	neural cell adhesion molecule 1
PDGFRB	5159	PDGFRB	platelet derived growth factor receptor beta
PECAM1	5175	PECAM1	platelet/endothelial cell adhesion molecule 1
T cell activation genes			
PRF1	5551	PRF1	perforin 1
GZMA	3001	GZMA	granzyme A
GZMB	3002	GZMB	granzyme B
Checkpoint T cell genes			
CD28	940	CD28	CD28 molecule
ENTPD1	953	ENTPD1 cd39	Ectonucleoside triphosphate diphosphohydrolase 1
NT5E	4907	NT5E cd73	5'-nucleotidase ecto
CD96	10225	CD96	CD96 molecule, TIGIT family
TIGIT	201633	TIGIT	T-cell immunoreceptor with Ig and ITIM domains
CD226	10666	CD226	CD226 molecule, TIGIT family

TNFRSF14	8764	TNFRSF14	tumor necrosis factor receptor superfamily member 14
TNFRSF18	8784	GITR	tumor necrosis factor receptor superfamily member 18
TNFRSF4	7293	OX-40, CD134	tumor necrosis factor receptor superfamily member 4
TNFRSF7	939	CD27	CD27 molecule
TNFRSF9	3604	CD137, 4-1BB	tumor necrosis factor receptor superfamily member 9
HAVCR2	84868	HAVCR2, Tim-3	hepatitis A virus cellular receptor 2
ICOS	29851	ICOS	inducible T-cell co-stimulator
LAG3	3902	LAG3	lymphocyte activating 3
PDCD1	5133	PDCD1	programmed cell death 1
Checkpoint tumor cell genes			
IDO1	3620	IDO1	indoleamine 2,3-dioxygenase 1
CD80	941	CD80, B7-1	CD80 molecule
CD86	942	CD86, B7-2	CD86 molecule
CD276	80381	CD276, B7H3, inhibitory	CD276 molecule
LGALS9	3965	LGALS9	lectin, galactoside-binding, soluble, 9
CD274	29126	CD274, PDL1	CD274 molecule
PDCD1LG2	80380	PDCD1LG2	programmed cell death 1 ligand 2

ICOSLG	23308	ICOSLG	inducible T-cell co-stimulator ligand
PVR	5817	PVR, CD155 (Tigit ligand)	poliovirus receptor
PVRIG	79037	PVRIG, CD112R	poliovirus receptor related immunoglobulin domain containing
TNFSF4	7292	OX40L	tumor necrosis factor superfamily member 4
Inferferon signature genes			
CXCL10	3627	CXCL10	C-X-C motif chemokine ligand 10
IFI27	3429	IFI27	interferon, alpha-inducible protein 27
IFI44L	10964	IFI44L	interferon induced protein 44 like
IFI6	2537	IFI6	interferon, alpha-inducible protein 6
IFIT1	3434	IFIT1	interferon induced protein with tetratricopeptide repeats 1
IRF8	3394	IRF8	interferon regulatory factor 8
MX1	4599	MX1	MX dynamin like GTPase 1
OAS1	4938	OAS1	2'-5'-oligoadenylate synthetase 1
RSAD2	91543	RSAD2	radical S-adenosyl methionine domain containing 2
G1P2	9636	ISG15	ISG15 ubiquitin-like modifier
Major histocompatibility complex genes			
HLA-A	3105	HLA-A	major histocompatibility complex, class I, A
HLA-B U3/L3	3106	HLA-B	major histocompatibility complex, class I, B
HLA-C U2/L2	3107	HLA-C	major histocompatibility complex, class I, C

HLA-DRA	3122	HLA-DRA	major histocompatibility complex, class II, DR alpha
HLA-DRB	3123	HLA-DRB1	major histocompatibility complex, class II, DR beta 1

Table 2: Clinico-pathological characteristics and survival of 42 NMIBC patients

	Whole population	No recurrence	Recurrence		Muscle-invasive progression	
	Number of patients (%)	Number (%)	Number (%)	p-value*	Number (%)	p-value**
Total population	42 (100)	13 (31.0)	21 (50.0)		8 (19.0)	
Age (years)						
≥60	33 (78.6)	9 (69.2)	16 (76.2)	0.96 (NS)	8 (100.0)	0.17 (NS)
<60	9 (21.4)	4 (30.8)	5 (23.8)		0 (0.0)	
Sex						
Male	39 (92.9)	12 (92.3)	19 (90.5)	>0.99 (NS)	8 (100.0)	>0.99 (NS)
Female	3 (7.1)	1 (7.7)	2 (9.5)		0 (0.0)	
Smoking status						
Non-smoker	17 (40.5)	3 (23.1)	11 (52.4)	0.092 (NS)	3 (37.5)	0.83 (NS)
Smoker	25 (59.5)	10 (76.9)	10 (47.6)		5 (62.5)	

History of NMIBC						
No	22 (52.4)	10 (76.9)	9 (42.9)	0.052 (NS)	3 (37.5)	0.59 (NS)
Yes	20 (47.6)	3 (23.1)	12 (57.1)		5 (62.5)	
Associated pTis						
No	40 (95.2)	13 (100.0)	21 (100.0)	>0.99 (NS)	6 (75.0)	**0.033**
Yes	2 (4.8)	0 (0.0)	0 (0.0)		2 (25.0)	
Grade						
Low grade	18 (42.9)	8 (61.5)	9 (42.9)	0.29 (NS)	1 (12.5)	0.13 (NS)
High grade	24 (57.1)	5 (38.5)	12 (57.1)		7 (87.5)	
Tumor stage [a]						
Ta	28 (68.3)	9 (69.2)	17 (81.0)	0.71 (NS)	2 (28.6)	**0.024**
T1	13 (31.7)	4 (30.8)	4 (19.0)		5 (71.4)	

* Chi^2 test, Chi^2 test with Yates' correction or Fisher test if appropriate (recurrence versus no recurrence)

** Chi^2 test, Chi^2 test with Yates' correction or Fisher test if appropriate (muscle-invasive progression versus others)

NS: not significant

[a] data available for 41 patients

Table 3: Clinico-pathological characteristics and survival of 56 MIBC patients

	Whole population	**Disease-free survival**		**Overall survival**	
	Number of patients (%)	**Number of events (%)**[a]	**p-value***	**Number of events (%)**[b]	**p-value***
Total population	56 (100.0)	36 (64.3)		34 (60.7)	
Age (years)					
≥60	40 (71.4)	30 (83.3)	**0.0082**	30 (88.2)	**0.0005**
<60	16 (28.6)	6 (16.7)		4 (11.8)	
Sex					
Male	42 (75.0)	24 (66.7)	0.053 (NS)	26 (76.5)	0.75 (NS)
Female	14 (25.0)	12 (33.3)		8 (23.5)	
Smoking status[c]					
Non-smoker	9 (18.0)	7 (23.3)	0.41 (NS)	7 (24.1)	0.34 (NS)
Smoker	41 (82.0)	23 (76.7)		22 (75.9)	
History of NMIBC					

No	35 (62.5)	21 (58.3)	0.39 (NS)	20 (58.8)	0.48 (NS)
Yes	21 (37.5)	15 (41.7)		14 (41.2)	
Associated pTis					
No	50 (89.3)	34 (94.4)	0.17 (NS)	32 (94.1)	0.20 (NS)
Yes	6 (10.7)	2 (5.6)		2 (5.9)	
Tumor stage					
T2	19 (33.9)	11 (30.6)	0.47 (NS)	8 (23.5)	**0.041**
≥T3	37 (66.1)	25 (69.4)		26 (76.5)	
Lymph node status[d]					
N-	35 (63.6)	18 (51.4)	**0.013**	17 (50.0)	**0.0075**
N+	20 (36.4)	17 (48.6)		17 (50.0)	
***FGFR3* status**					
Mutated	6 (10.7)	4 (11.1)	>0.99 (NS)	4 (11.8)	>0.99 (NS)
Not mutated	50 (89.3)	32 (88.9)		30 (88.2)	
***PIK3CA* status**					
Mutated	6 (10.7)	2 (5.6)	0.17 (NS)	2 (5.9)	0.20 (NS)
Not mutated	50 (89.3)	34 (94.4)		32 (94.1)	

* Chi^2 test, Chi^2 test with Yates' correction or Fisher test if appropriate

NS: not significant

[a] first recurrence (local or metastatic)

[b] death

[c] data available for 50 patients

[d] data available for 55 patients

Table 4: List of the evaluated 36 genes coding for human chemokines and integrins

ID	GeneID	GeneSymbol	GeneName
Chemokines genes			
CCL2	6347	CCL2	C-C motif chemokine ligand 2
CCL3	6348	CCL3	C-C motif chemokine ligand 3
CCL4	6351	CCL4	C-C motif chemokine ligand 4
CCL5	6352	CCL5	C-C motif chemokine ligand 5
CCL8	6355	CCL8	C-C motif chemokine ligand 8

CCL21	6366	CCL21	C-C motif chemokine ligand 21
CSF2	1437	CSF2	colony stimulating factor 2
CX3CL1	6376	CX3CL1	C-X3-C motif chemokine ligand 1
CXCL1	2919	CXCL1	C-X-C motif chemokine ligand 1
CXCL2	2920	CXCL2	C-X-C motif chemokine ligand 2
CXCL3	2921	CXCL3	C-X-C motif chemokine ligand 3
CXCL5	6374	CXCL5	C-X-C motif chemokine ligand 5
CXCL6	6372	CXCL6	C-X-C motif chemokine ligand 6
CXCL9	4283	CXCL9	C-X-C motif chemokine ligand 9
CXCL10	3627	CXCL10	C-X-C motif chemokine ligand 10
CXCL11	6373	CXCL11	C-X-C motif chemokine ligand 11
CXCL12	6387	CXCL12	C-X-C motif chemokine ligand 12
CXCL13	10563	CXCL13	C-X-C motif chemokine ligand 13
Adhesion molecules genes			
ITGA1	3672	ITGA1	integrin subunit alpha 1/ CD49a/ VLA1
ITGA2	3673	ITGA2	integrin subunit alpha 2
ITGA4	3676	ITGA4	integrin subunit alpha 4
ITGA5	3678	ITGA5	integrin subunit alpha 5
ITGA6	3655	ITGA6	integrin subunit alpha 6
ITGAV	3685	ITGAV	integrin subunit alpha V
ITGB1	3688	ITGB1	integrin subunit beta 1
ITGB3	3690	ITGB3	integrin subunit beta 3
ITGB4	3691	ITGB4	integrin subunit beta 4
ITGB5	3693	ITGB5	integrin subunit beta 5

ITGB8	3696	ITGB8	integrin subunit beta 8
ICAM1	3383	ICAM1	intercellular adhesion molecule 1
ITGAM	3684	ITGAM	integrin subunit alpha M
SELE	6401	SELE	selectin E
VCAM1	7412	VCAM1	vascular cell adhesion molecule 1
Angiogenesis involved genes			
VEGF	7422	VEGFA	vascular endothelial growth factor A
VEGFB	7423	VEGFB	vascular endothelial growth factor B
VEGFC	7424	VEGFC	vascular endothelial growth factor C

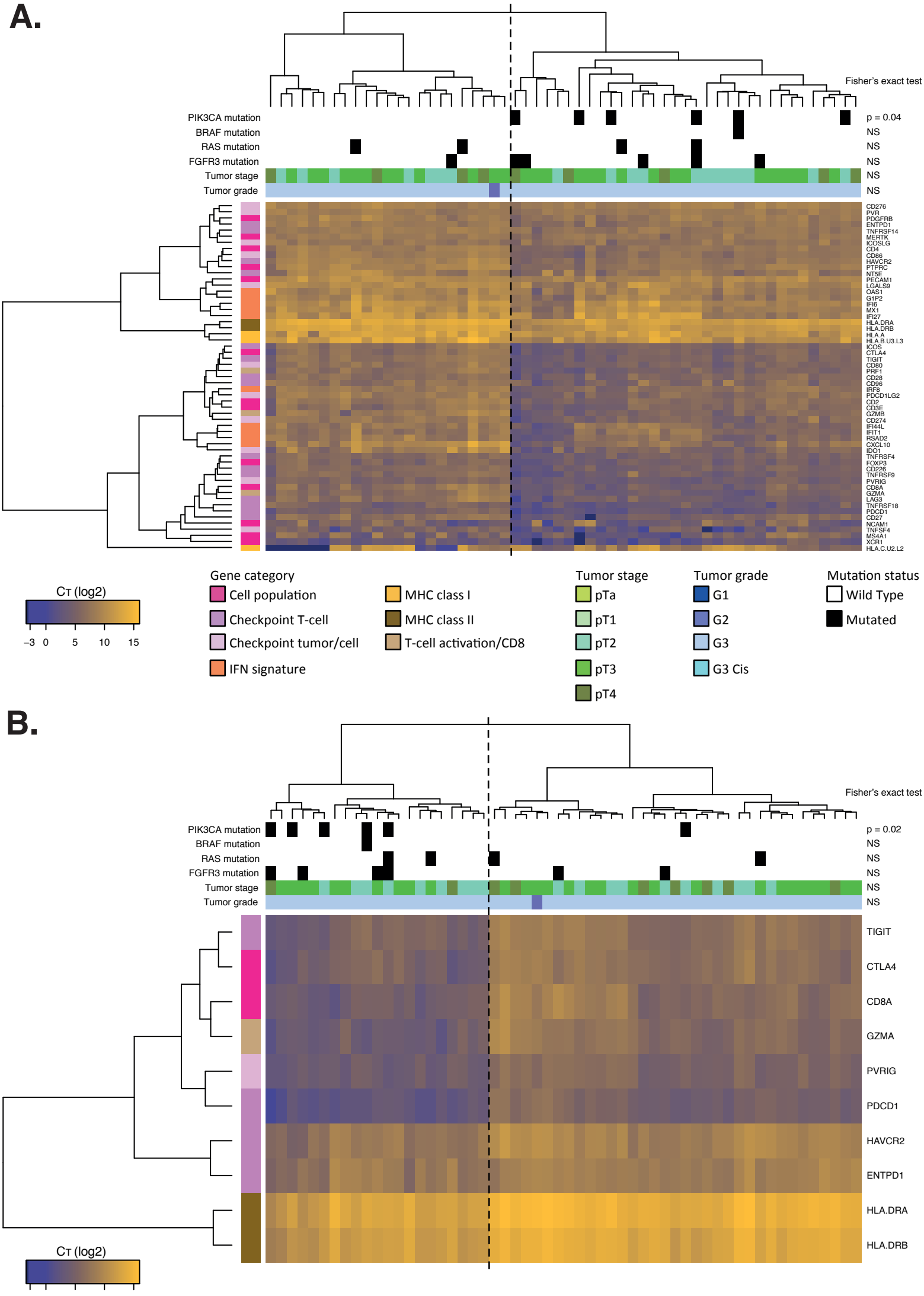
A.
Fisher's exact test
PIK3CA mutation
BRAF mutation
RAS mutation
FGFR3 mutation
Tumor stage
Tumor grade
p = 0.04
NS
NS
NS
NS
NS
CD276
PVR
PDGFRB
ENTPD1
TNFRSF14
MERTK
ICOSLG
CD4
CD86
HAVCR2
PTPRC
NT5E
PECAM1
LGALS9
OAS1
G1P2
IFI6
MX1
IFI27
HLA.DRA
HLA.DRB
HLA.A
HLA.B.U3.L3
ICOS
CTLA4
TIGIT
CD80
PRF1
CD28
CD96
IRF8
PDCD1LG2
CD2
CD3E
GZMB
CD274
IFI44L
IFIT1
RSAD2
CXCL10
IDO1
TNFRSF4
FOXP3
CD226
TNFRSF9
PVRIG
CD8A
GZMA
LAG3
TNFRSF18
PDCD1
CD27
NCAM1
TNFSF4
MS4A1
XCR1
HLA.C.U2.L2
CT (log2)
−3 0 5 10 15
Gene category
Cell population
Checkpoint T-cell
Checkpoint tumor/cell
IFN signature
MHC class I
MHC class II
T-cell activation/CD8
Tumor stage
pTa
pT1
pT2
pT3
pT4
Tumor grade
G1
G2
G3
G3 Cis
Mutation status
Wild Type
Mutated
B.
Fisher's exact test
PIK3CA mutation
BRAF mutation
RAS mutation
FGFR3 mutation
Tumor stage
Tumor grade
p = 0.02
NS
NS
NS
NS
NS
TIGIT
CTLA4
CD8A
GZMA
PVRIG
PDCD1
HAVCR2
ENTPD1
HLA.DRA
HLA.DRB
CT (log2)
−3 0 5 10 15

Figure 1.

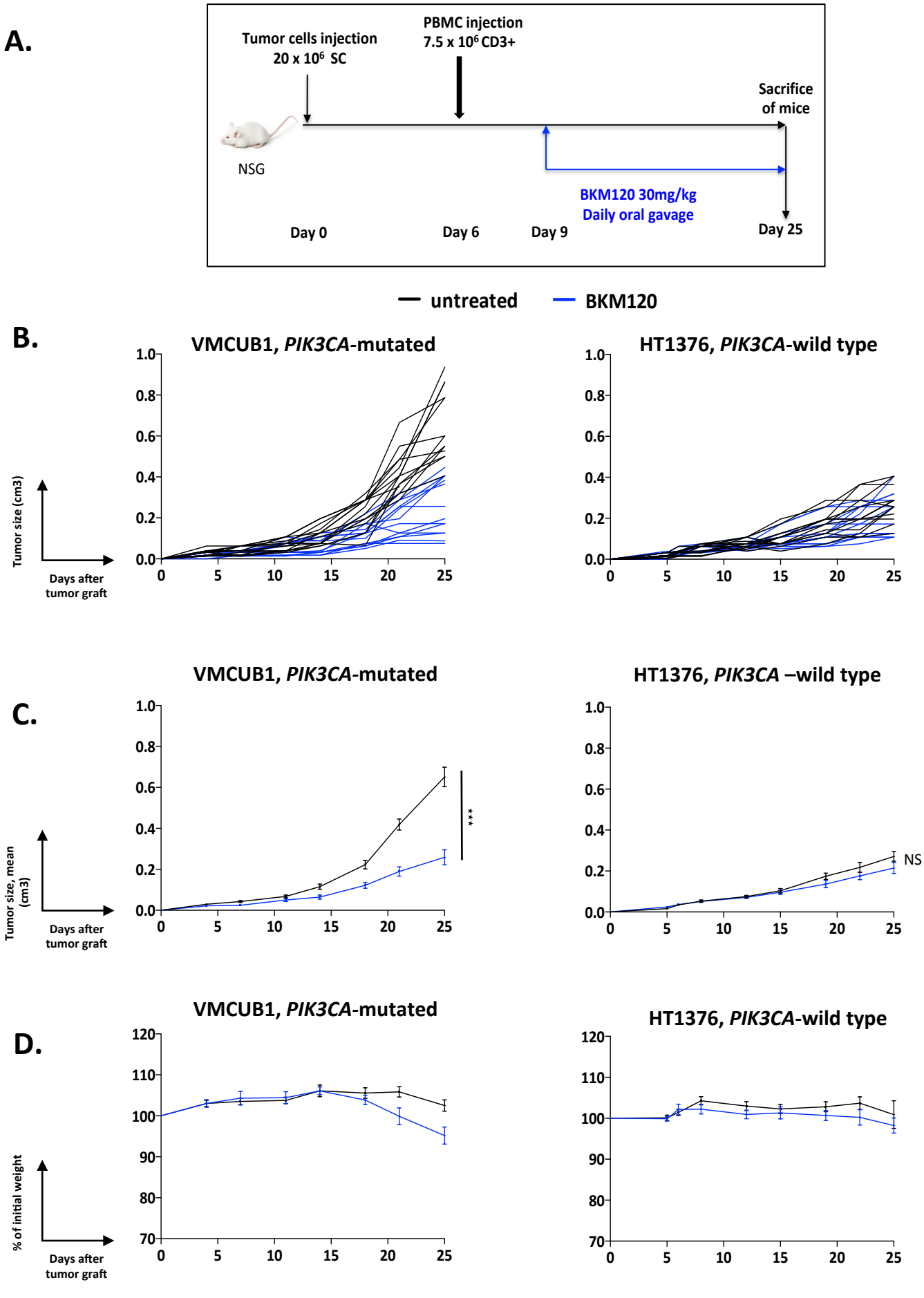
A.
Tumor cells injection
20 x 10⁶ SC
PBMC injection
7.5 x 10⁶ CD3+
Sacrifice
of mice
NSG
BKM120 30mg/kg
Daily oral gavage
Day 0
Day 6
Day 9
Day 25
untreated
BKM120
B.
VMCUB1, PIK3CA-mutated
HT1376, PIK3CA-wild type
Tumor size (cm3)
Days after
tumor graft
C.
VMCUB1, PIK3CA-mutated
HT1376, PIK3CA –wild type
Tumor size, mean
(cm3)
***
NS
D.
VMCUB1, PIK3CA-mutated
HT1376, PIK3CA-wild type
% of initial weight

Figure 2.

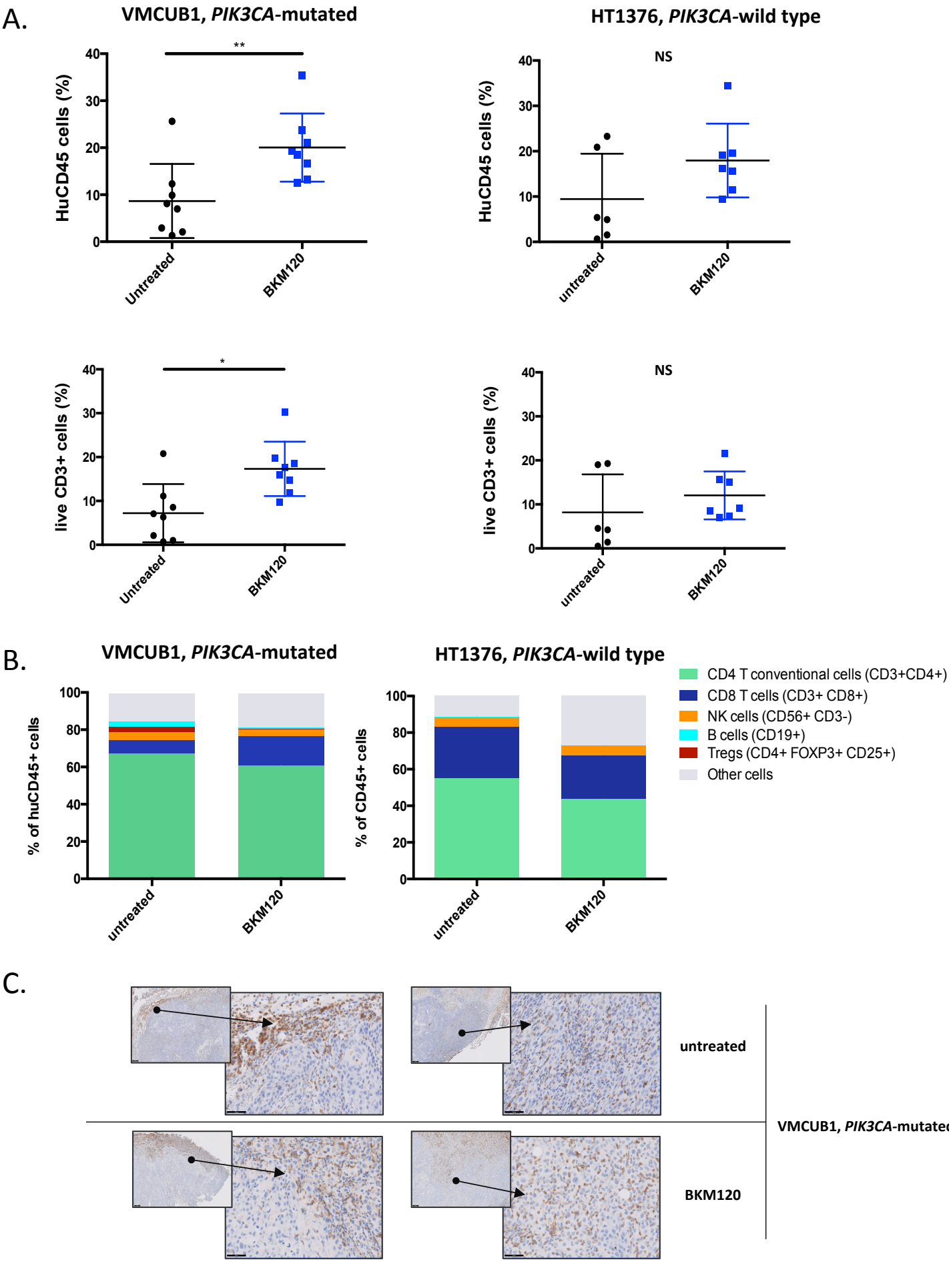
A.
VMCUB1, PIK3CA-mutated
HT1376, PIK3CA-wild type
HuCD45 cells (%)
live CD3+ cells (%)
**
*
NS
Untreated
BKM120
untreated
B.
% of huCD45+ cells
% of CD45+ cells
CD4 T conventional cells (CD3+CD4+)
CD8 T cells (CD3+ CD8+)
NK cells (CD56+ CD3-)
B cells (CD19+)
Tregs (CD4+ FOXP3+ CD25+)
Other cells
C.
untreated
BKM120
VMCUB1, PIK3CA-mutated

Figure 3.

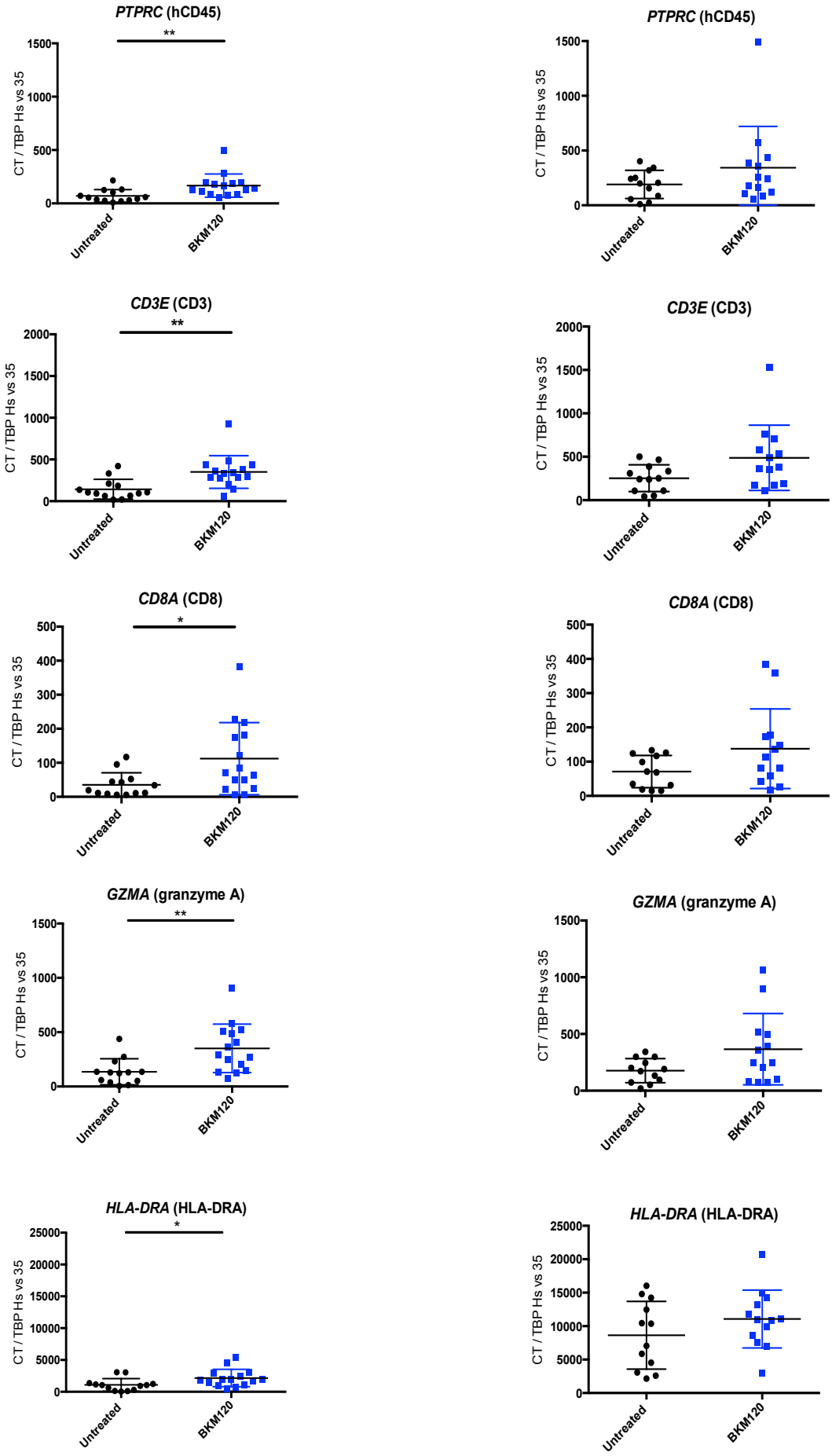
VMCUB1, PIK3CA-mutated
HT1376, PIK3CA-wild type
PTPRC (hCD45)
CD3E (CD3)
CD8A (CD8)
GZMA (granzyme A)
HLA-DRA (HLA-DRA)
CT / TBP Hs vs 35
Untreated
BKM120
**
*

Figure 4.

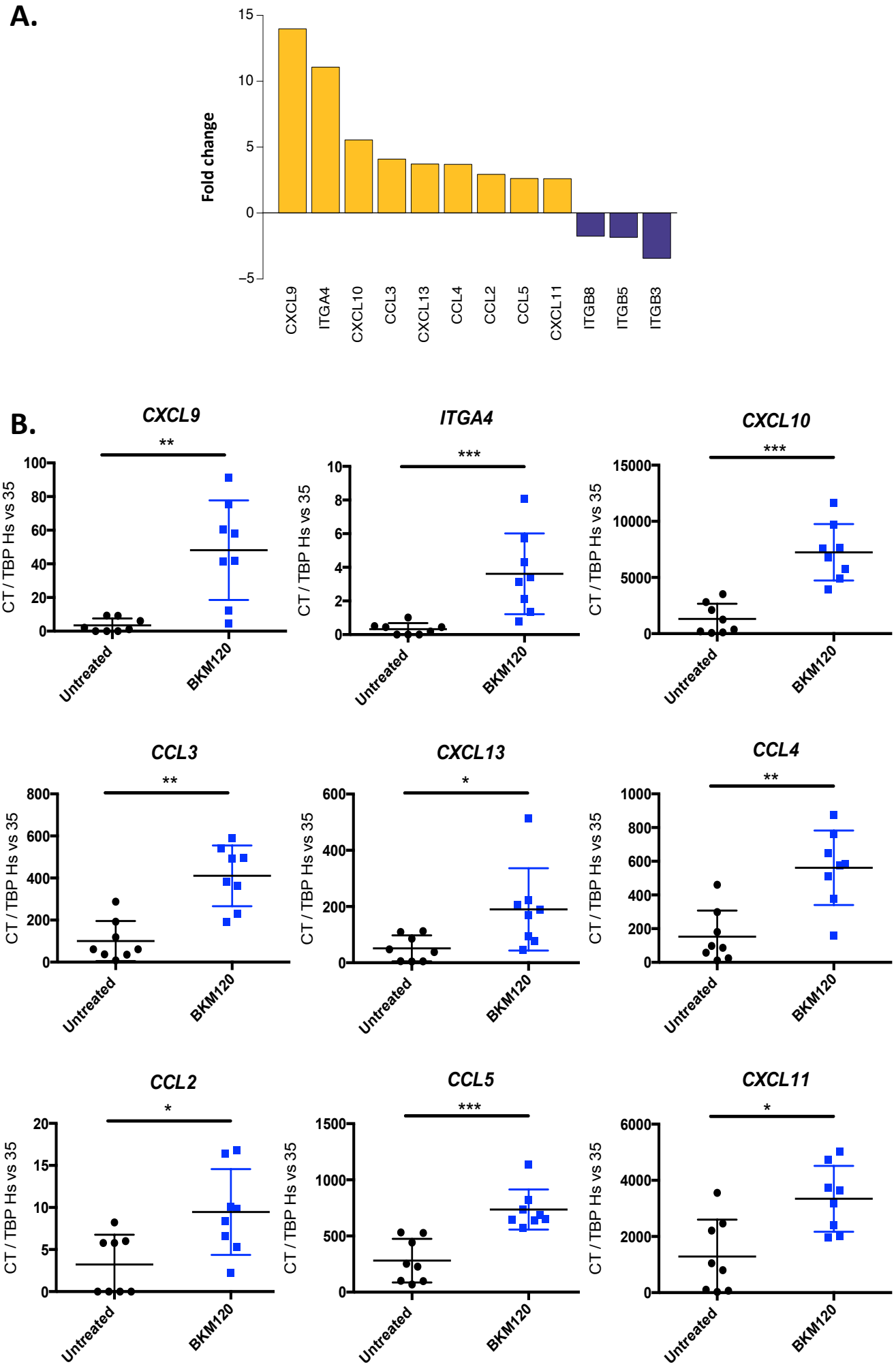
A.
Fold change
15
10
5
0
−5
CXCL9
ITGA4
CXCL10
CCL3
CXCL13
CCL4
CCL2
CCL5
CXCL11
ITGB8
ITGB5
ITGB3
B.
CXCL9
ITGA4
CXCL10
CCL3
CXCL13
CCL4
CCL2
CCL5
CXCL11
CT / TBP Hs vs 35
Untreated
BKM120
**
***
*

Figure 5.

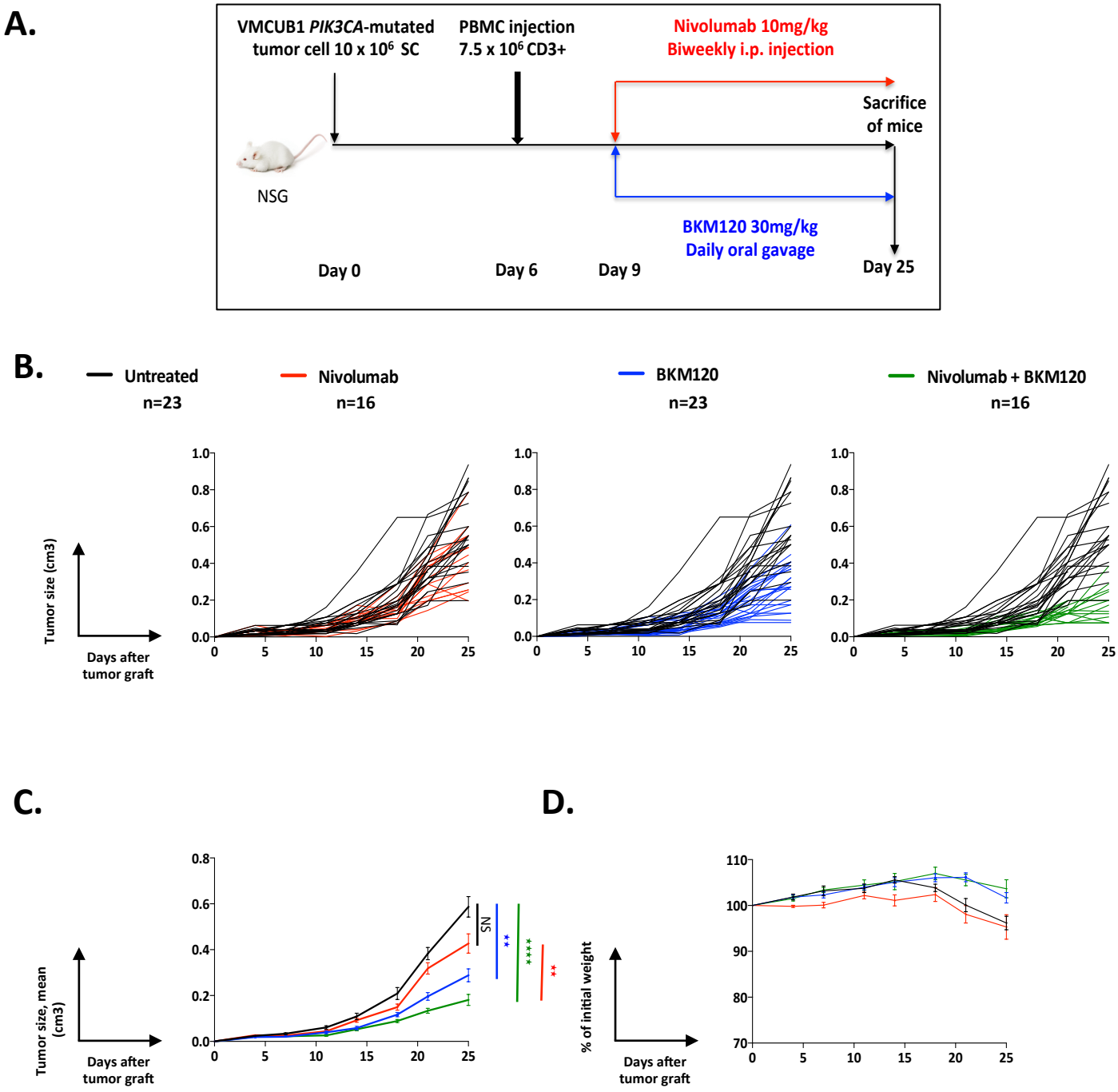
A.
VMCUB1 PIK3CA-mutated tumor cell 10 x 10^6 SC
PBMC injection 7.5 x 10^6 CD3+
Nivolumab 10mg/kg Biweekly i.p. injection
Sacrifice of mice
NSG
BKM120 30mg/kg Daily oral gavage
Day 0
Day 6
Day 9
Day 25
B.
Untreated n=23
Nivolumab n=16
BKM120 n=23
Nivolumab + BKM120 n=16
Tumor size (cm3)
Days after tumor graft
C.
Tumor size, mean (cm3)
Days after tumor graft
NS
**
****
**
D.
% of initial weight
Days after tumor graft

Figure 6.

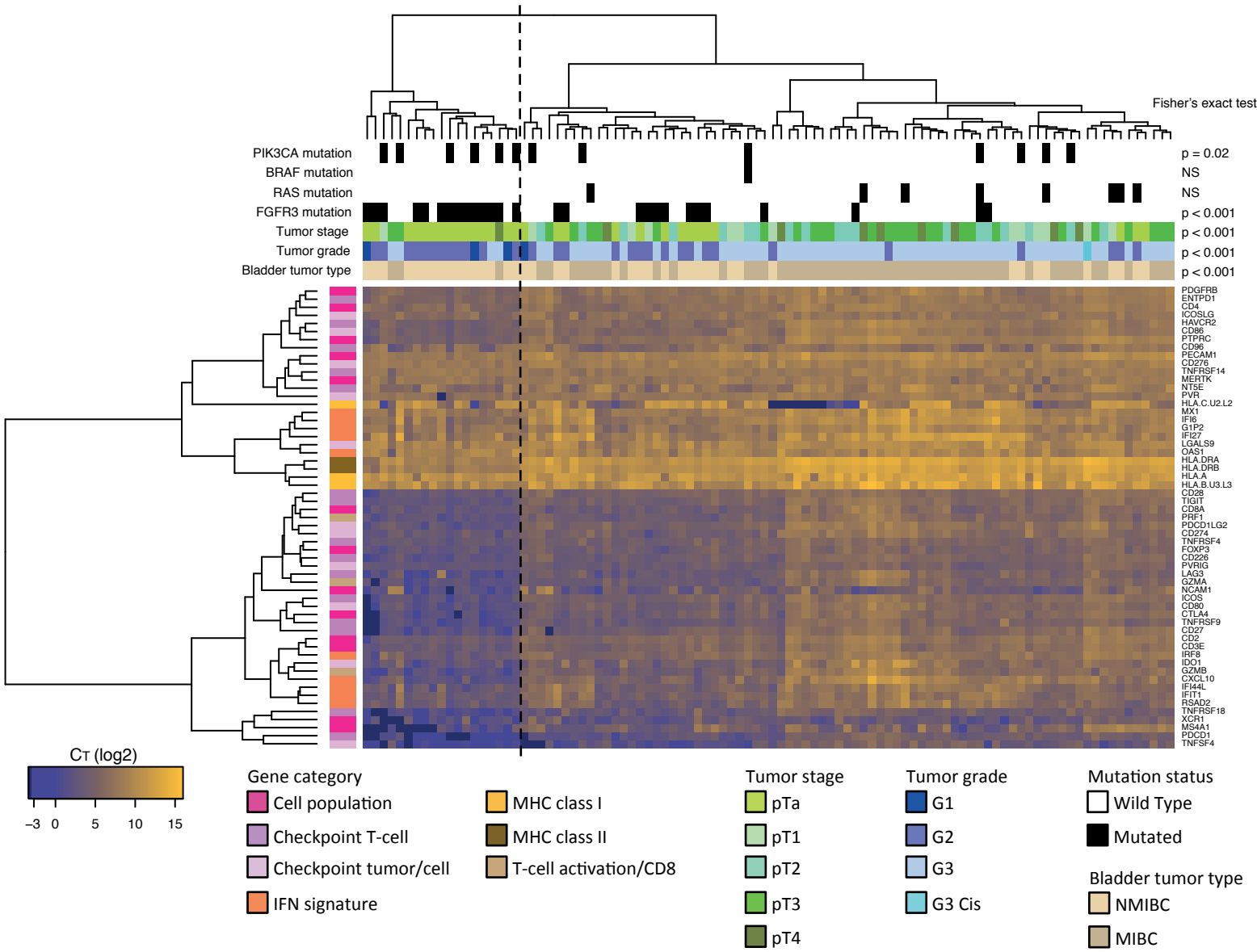

Supplementary Figure 1.

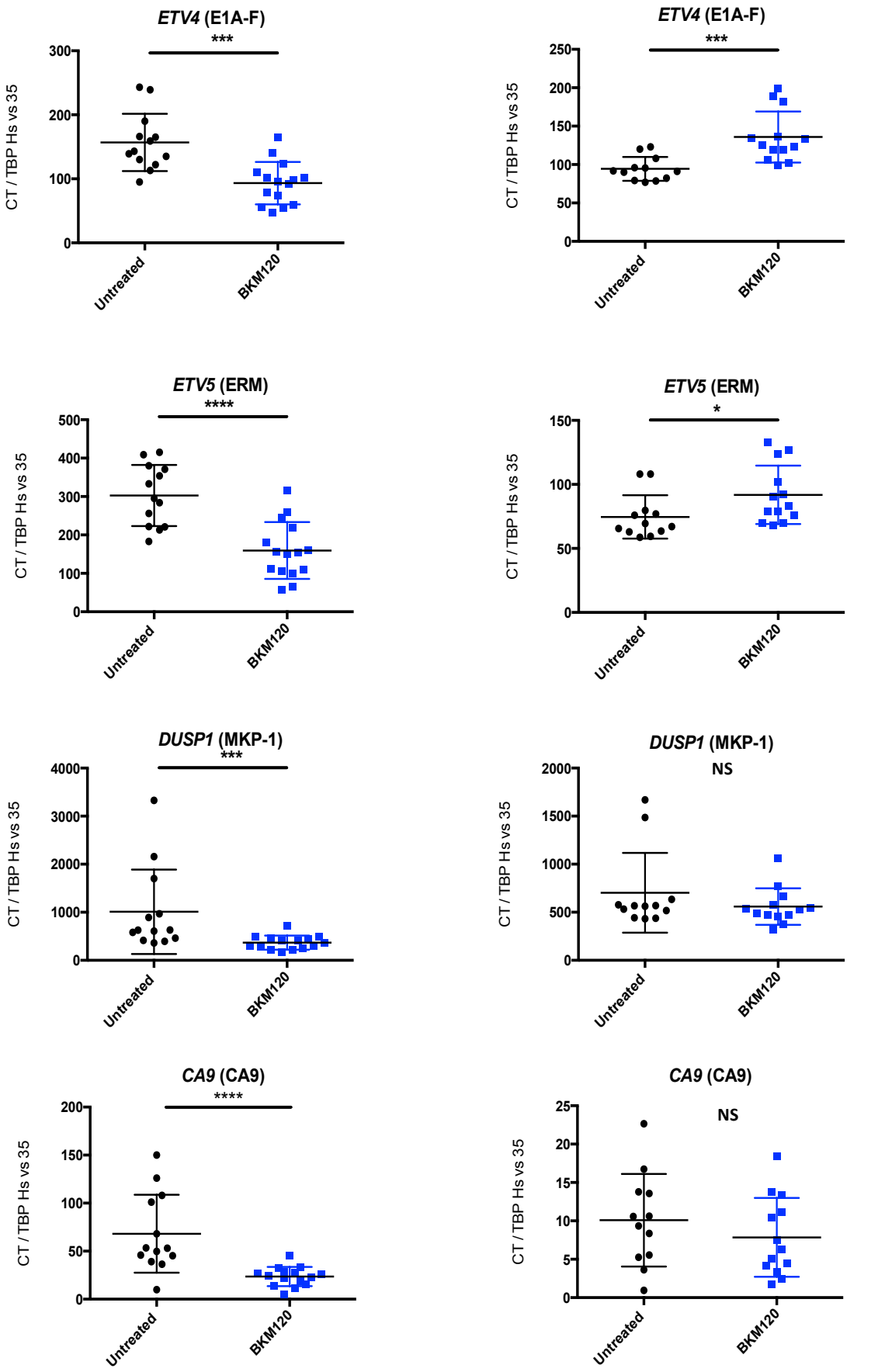

Supplementary Figure 2.

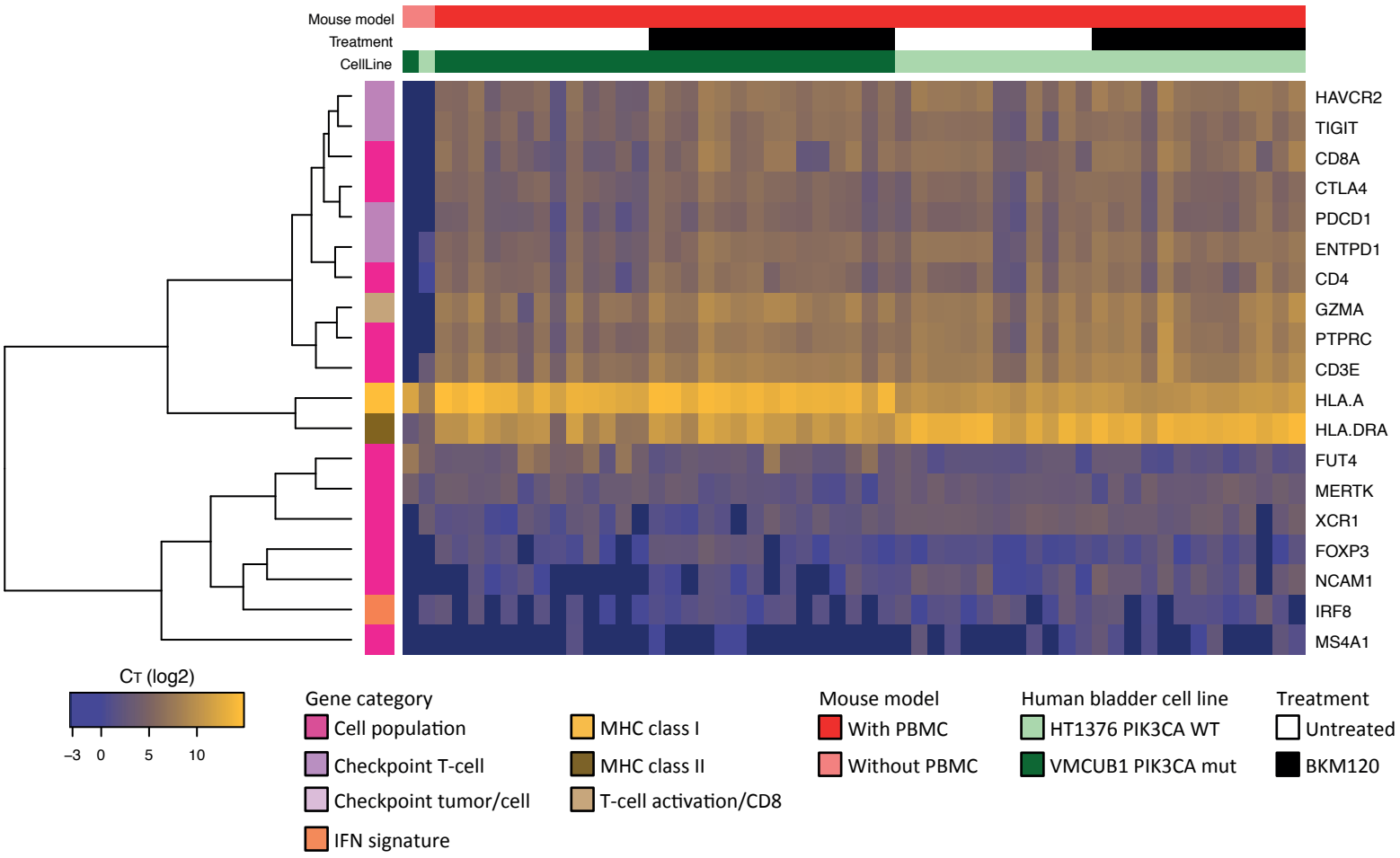

Supplementary Figure 3.

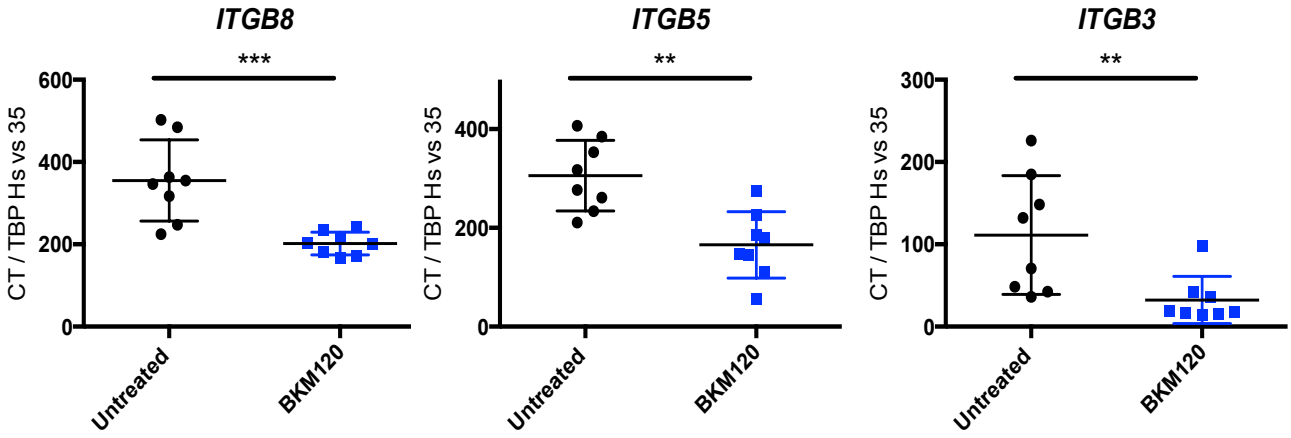

Supplementary Figure 4.

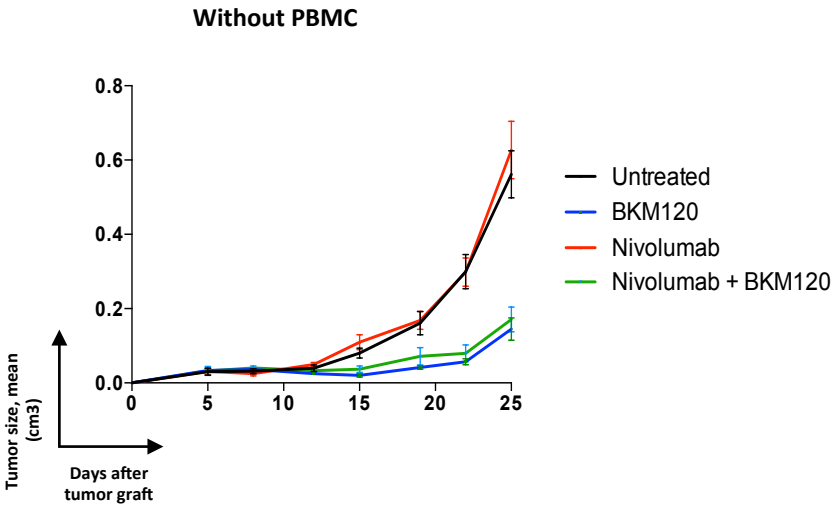

Supplementary Figure 5.